VeriMask: Facilitating Decontamination of N95 Masks in the COVID-19 Pandemic: Challenges, Lessons Learned, and Safeguarding the Future

YAN LONG, EECS Department, University of Michigan, USA
ALEXANDER CURTISS, ECE Department, Northwestern University, USA
SARA RAMPAZZI, CISE Department, University of Florida, USA
JOSIAH HESTER, ECE & CS Department, Northwestern University, USA
KEVIN FU, EECS Department, University of Michigan, USA

The US CDC has recognized moist-heat as one of the most effective and accessible methods of decontaminating N95 masks for reuse in response to the persistent N95 mask shortages caused by the COVID-19 pandemic. However, it is challenging to reliably deploy this technique in healthcare settings due to a lack of smart technologies capable of ensuring proper decontamination conditions of hundreds of masks simultaneously. To tackle these challenges, we developed an open-source wireless sensor platform—VeriMask[1] —that facilitates per-mask verification of the moist-heat decontamination process. VeriMask is capable of monitoring hundreds of masks simultaneously in commercially available heating systems and provides a novel throughput-maximization functionality to help operators optimize the decontamination settings. We evaluate VeriMask in laboratory and real-scenario clinical settings and find that it effectively detects decontamination failures and operator errors in multiple settings and increases the mask decontamination throughput. Our easy-to-use, low-power, low-cost, scalable platform integrates with existing hospital protocols and equipment, and can be broadly deployed in under-resourced facilities to protect front-line healthcare workers by lowering their risk of infection from reused N95 masks. We also memorialize the design challenges, guidelines, and lessons learned from developing and deploying VeriMask during the COVID-19 Pandemic. Our hope is that by reflecting and reporting on this design experience, technologists and front-line health workers will be better prepared to collaborate for future pandemics, regarding mask decontamination, but also other forms of crisis tech.

CCS Concepts: • **Computer systems organization → Embedded systems**.

Additional Key Words and Phrases: Wireless Sensor, COVID-19, N95 Masks Decontamination

ACM Reference Format:
Yan Long, Alexander Curtiss, Sara Rampazzi, Josiah Hester, and Kevin Fu. 2021. VeriMask: Facilitating Decontamination of N95 Masks in the COVID-19 Pandemic: Challenges, Lessons Learned, and Safeguarding the Future. *Proc. ACM Interact. Mob. Wearable Ubiquitous Technol.* 5, 3, Article 119 (September 2021), 29 pages. https://doi.org/10.1145/3478105

[1]We release our open-source design at https://github.com/longyan97/VeriMask_Designs

Authors' addresses: Yan Long, EECS Department, University of Michigan, Ann Arbor, Michigan, USA, yanlong@umich.edu; Alexander Curtiss, ECE Department, Northwestern University, Evanston, Illinois, USA, alexandercurtiss2025@u.northwestern.edu; Sara Rampazzi, CISE Department, University of Florida, Gainesville, Florida, USA, srampazzi@ufl.edu; Josiah Hester, ECE & CS Department, Northwestern University, Evanston, Illinois, USA, josiah@northwestern.edu; Kevin Fu, EECS Department, University of Michigan, Ann Arbor, Michigan, USA, kevinfu@umich.edu.

2474-9567/2021/9-ART119 $15.00
https://doi.org/10.1145/3478105

1 INTRODUCTION

N95 mask shortages have been a persistent and enduring problem in almost every significant pandemic. The SARS outbreaks in 2003, H1N1 influenza in 2009 [60, 100], and the COVID-19 pandemic all had severe N95 shortages. During each pandemic, the abrupt and fierce increase in the demand for N95 masks quickly depleted the supply chain, forcing the public and healthcare workers to reuse their masks. The ongoing COVID-19 pandemic has seen particularly serious and prolonged N95 mask shortages worldwide. For instance, a survey in the US from early 2020 [29] shows that over 50% of 21,000 nurses surveyed were required to reuse N95 masks for at least 5 days on average. The mask shortage has been plaguing the US even until early 2021 [16, 35] and has continued to severely impact India [11, 38] and other countries [34, 37] suffering from the new wave of COVID-19 variants. The reuse of N95 masks poses severe risk of infection because of the potential pathogenic agents present on the masks, especially for front-line healthcare workers using the same disposable mask over multiple days when treating patients [31].

While these cycles of N95 shortages in recent pandemics highlight the poor preparedness of personal protection equipment (PPE) supply chain management [60, 100], it also raises a question for researchers and system developers: What can be done in a pandemic to quickly respond to N95 mask shortages, and how can researchers engage with communities to prepare for future shortages in the next pandemic? The medical research community has proposed several methods for decontaminating single-use N95 masks for safe reuse, such as hydrogen peroxide dosing, autoclave treatment, gamma and UV-C irradiation, etc [101]. These methods, however, either suffer from chemical exposure and potential harm to the wearer caused by toxic residuals [30], or require expensive specialized equipment costing as much as $6 million USD [25].

In this work, we identify a candidate for safe, low-cost, and efficient N95 mask decontamination, i.e., the moist-heat decontamination method, and study the critical challenges preventing this decontamination method from being rapidly, widely, and reliably deployed in healthcare facilities for protecting front-line healthcare workers. Moist-heat decontamination has been recognized by the US CDC as one of the most effective and easy-to-operate decontamination methods for the SARS-CoV-2 virus [18], and has the potential to be deployed using commercial heating devices such as ovens and warming cabinets that are already widely available in hospitals [17]. Such deployment, however, is challenging because of:

(1) the risks of decontamination failures caused by non-uniform heating and humidity fluctuations in the commercial heating systems [45, 78, 80],
(2) unpredictable operating errors, due to human error stemming from complex protocols and exhaustion,
(3) the large burden and difficulty of manual verification of each mask's decontamination status,
(4) and the impracticality of employing closed-loop control to achieve maximal decontamination throughput.

To address these challenges, we developed **VeriMask**, an open-source[2] wireless sensor platform that enables rapid, reliable, and cost-efficient moist-heat decontamination in healthcare facilities. VeriMask incorporates low-cost BLE-enabled sensor nodes in a dense sensing topology that continuously monitors the temperature and relative humidity of each mask and an Android application that is capable of automatically verifying the decontamination status of hundreds of masks simultaneously. Based on decontamination profiling, the Android application is also able to determine and suggest the optimal decontamination settings and help the operators to maximize the decontamination throughput. In order to be applicable in a wide range of decontamination scenarios and heating devices, VeriMask is designed to be flexible in terms of configurable decontamination parameters. VeriMask integrates with existing clinical workflows, and the wireless feature ensures scalability of VeriMask so that it can be rapidly deployed in clinical settings at large scales. The easy-to-use VeriMask App provides decontamination information of each individual mask and guarantees adequate decontamination before the N95 masks can be reused. The low-power, high temperature resistant clinical-use VeriMask sensor nodes with a size

[2]We release our open-hardware and open-source design at https://github.com/longyan97/VeriMask_Designs.

of 3.5 x 3.8 cm (1.4 x 1.5 inches) can work continuously for over 1000 decontamination cycles without change of battery and only cost $15.66 each at a quantity of 1000. We evaluated VeriMask in both a laboratory setting and a clinical setting. Results show that VeriMask is able to detect subtle decontamination failures that might go undetected without accurate verification and enhance efficiency by increasing decontamination throughput.

VeriMask creates a new system using well-known and verified components, which enables it to have a real impact on real-world clinics. VeriMask is the first realization of an open-source sensor system design for disposable mask decontamination, which can play critical roles in mitigating mask shortage emergency caused by current and future pandemics. To ensure that the challenges, lessons, and design outcomes from VeriMask's design and methodology can transfer to future open-source design for emergency response, we constructed a design framework from VeriMask's design criteria by relating to researches and works of Free and Open Source Hardware (FOSH) and proposed general design goals that can be widely applied. Finally, we glean lessons from our experience with building and deploying VeriMask, and the experience of our clinical and near-clinical collaborators and partners. We envision that our highly adaptable open-source VeriMask platform and our experience can greatly accelerate the design and deployment process of mask decontamination sensor systems and safeguard society when the next pandemic hits. We hope that the general lessons learned from mobile computing researchers responding to a societal-scale emergency will be memorialized and aid future researches hoping to respond to future crises. We summarize our main contributions as follows:

(1) We designed and built the VeriMask platform specifically conceived to verify moist-heat decontamination processes of N95 masks in a semi-automated, human-in-the-loop, reliable way. VeriMask is flexible, scalable, low-power, and easy-to-use for non-specialized operators, which enables rapid deployment in under-resourced clinical settings to protect front-line health workers. VeriMask is self-healing and adjusts to diverse types of heating devices using a profiling function and operator feedback.
(2) We evaluate VeriMask in laboratory and clinical settings and demonstrate its effectiveness in detecting unsuccessful decontamination that might remain undetected using conventional approaches. We also integrate VeriMask into existing emergency operating protocols to enable fast, low-cost, and reliable deployment of moist-heat decontamination processes with commercial heating devices in hospitals.
(3) We formulate VeriMask's design criteria in a transferable way and elaborate our design experience, considerations, and lessons learned to help future designers quickly respond to mask shortage (and other large-scale societal) emergencies with open-source design.

2 BACKGROUND & RELATED WORK

2.1 N95 Masks Decontamination Methods

Disposable N95 Filtering Facepiece Respirators (FFRs) commonly referred to as N95 masks or N95 respirators, are worn by healthcare workers for self-protection. These masks are composed of multiple layers including an electrostatic filter, depending on the model. With more than 95% filtration efficiency, they are designed to prevent the wearer from inhaling small airborne particles by capturing them via mechanical and electrostatic forces [1, 20]. N95 respirators are "single-use," disposable devices that should not be shared or reused.

The US Centers for Disease Control and Prevention (CDC) indicates that N95 masks can be used for up to 8 hours (including between patients), then the device should be properly discarded and replaced [24]. Over time, the warm and humid environment caused by breathing can accelerate the spread of the captured microorganisms to the inner layers of the mask, posing a risk of contaminant exposure for the wearer [99].

The shortage of N95 masks during the SARS-CoV-2 pandemic has prompted the consideration of reuse of these devices after a decontamination process to extend limited stocks [18]. The US Food and Drug Administration (FDA) guidance identifies as a target for adequate decontamination a 3-log level, or more, bioburden reduction. In other words the process should reach a viral load reduction of at least a factor of 1000 [26]. In addition, an

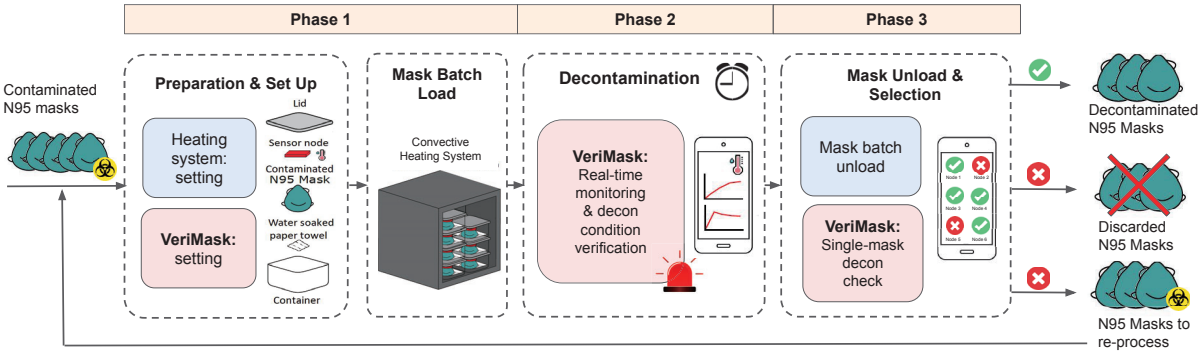

Fig. 1. Three phases of a typical moist-heat decontamination cycle integrated with VeriMask. *Phase 1:* Each contaminated mask is put into a rigid container with a VeriMask device and water soaked paper towel to create adequate humidity. Each sealed container is then transferred into the heating system. *Phase 2:* The Android app monitors the decontamination process in real time to detect potential anomalies (e.g. a container temperature dropped below threshold). *Phase 3:* After the decontamination time the operator check the type of failure flagged by VeriMask. If the masks that have experienced decontamination failure can be re-processed, they will be integrated in the next decontamination cycle, otherwise they will be discarded.

effective N95 mask decontamination should maintain the fit, sealing capacity, and the filtration performance of the mask. Finally, the process should not damage the mask's structural integrity, material, and should present no residual chemical hazard for the wearer due to the treatment (e.g. skin irritation, respiratory distress) [18].

Different approaches has been investigated to decontaminate disposable N95 masks to mitigate the shortage due to the massive demand, as shown in Table 1. In particular, the US National Institute for Occupational Safety and Health (NIOSH) [18] and teams of researchers [39, 57, 90, 93] have identified Ultraviolet Germicidal Irradiation (UVGI), hydrogen peroxide, and moist-heat (MH) as the most promising methods to decontaminate N95 masks against the virus SARS-CoV-2 without affecting the filtration capacity, fit, and seal.

While Hydrogen peroxide-based methods are widely used in hospitals for inactivating highly resistant pathogens [101], these processes require expensive and specialized equipment [25] and careful control of humidity level, gas saturation, concentration, and duration of exposure. The entire process has a duration up to 8 hours, and only trained personnel should operate the equipment because errors in the dosing protocols could result in decontamination failure and even explosion hazards [90]. In addition, hydrogen peroxide gas is a corrosive irritant that can interact with N95 mask to form toxic residues to wearers if not properly removed after treatment [15]. UVGI-based methods depends critically on the UV-C source wavelength (200-280 nm with peak efficacy at ~254 nm) and UV-C dose ($\geq$1.0 J/cm^2) applied to each mask surface [57]. Previous studies [61, 73, 103] have found that (i) the layer structure of certain N95 mask models and the presence of shadows can compromise the efficacy of the treatment because the mask surfaces may not receive the full UV-C dose, (ii) the mask straps required a further decontamination procedure because of residuals, (iii) direct exposure to UV-C light is harmful and UV wavelengths in the range of 175–210 nm can generate ozone which is hazardous to human health.

In contrast to hydrogen peroxide and UVGI methods, moist-heat treatments have minimal duration (typically 30-60 minute), do not require specialized and expensive equipment or a separate decontamination procedure for the straps, and do not require an off-gas time or a further treatment for removing dangerous chemical residues [39, 48, 79, 92]. For these reasons, MH methods can be suitable for wide and fast deployment in hospitals, laboratories, and non-specialized healthcare facilities that are generally already equipped with commercial

Table 1. Comparison between different N95 masks decontamination methods for on-site deployment. Moist-heat decontamination does not require expensive equipment or off-gas time to remove harmful gas or chemical residues.

Decontamination Method	Chemical Residue	Operator Hazard*	Process Time	Costs**	Throughput (N95/Cycle)	Max Reuse Cycles	Literature sources
VHP	Yes	Chemical	4-8h	$$$	≤ 160	4^{+}	[12, 19]
HPGP	Yes	Chemical	24min-1h	$$$	≤ 10	2^{+}	[13, 19]
UVGI	No	Ozone Exposure	10min***	$$	$\leq 30^{++}$	5	[10, 32]
Autoclave Steam	No	No	30min-1h	$$$$	12-20	4^{+}	[28, 44]
Moist Heat	No	No	30min-1h	$	$\leq 100^{++}$	5	[19, 39]

*Assuming standard protection procedures are followed (e.g. wearing mask, gloves, long-sleeved gown, eye protection).

**Considering startup and recurring costs: $$$$ = >$30,000, $$$ = $5,000 - $30,000, $$ = $1,000 - $5,000, $ = <$1,000.

***Dependent on bulb irradiance to ensure $\geq 1 J/cm^2$ dose is applied to each mask.

+Authorized under FDA Emergency Use Authorization (EUA) in Jan 2021. ++ Depending on the cabin dimension.

heating devices such as warming cabinets, environmental chambers, and convection ovens, which can achieve the required conditions.

2.2 WSNs For Environmental Monitoring

The design of the VeriMask wireless sensor platform falls into the category of wireless sensor networks (WSN) for environmental conditions monitoring. Such technology has been widely applied in fields like healthcare mointoring [40, 50, 65, 88], agricultural science [63, 68, 71, 83, 95], food processing [66, 94], and building monitoring [42, 55, 87]. Generally, WSN for environmental monitoring proposed in literature are highly application-specific, thus less adaptable to be utilized in masks decontamination processes [59, 67, 77]. Since most of the proposed platforms are not designed for harsh working conditions (e.g., the high operating temperature required in the MH process), they are likely to experience large performance decrease and even system malfunctions when deployed in a harsh environment. For instance, previous studies [41, 74] show that WSNs not specifically designed for high temperatures see sharp decreases in wireless signal strength when temperature increases, leading to aggravated packet loss and energy consumption. In addition, many of these previous WSNs require long wireless transmission range of up to 100 meters [68, 94]. Compared to our close-distance monitoring application scenario, they consume extra power to boost signal strength. Sisinni et al. [98] designed a wireless temperature monitoring network for autoclave steam sterilizers. However, their proposed network is specialized for high-pressure autoclave temperature monitoring and not suitable for convection oven-based temperature and humidity verification. In addition, the high sample rate and other specific requirements for steam sterilizers result in an average power consumption of 0.4 mA, as well as a larger size platform, making it not compatible with the N95 mask MH decontamination requirements [39]. VeriMask, in contrast, is conceived for real-time moist-heat decontamination processes verification that can be used widely on generic convection heating systems.

According to our research, currently there exists no commercial wireless temperature and RH monitoring systems that satisfy the high-temperature requirement (up to 90°C) of MH decontamination and are as scalable and automated as VeriMask. Typical wireless sensors on the market [27] can only operate under 60°C, and uses WiFi or Bluetooth synchronous communication for data transmission which requires additional time for establishing the connection and limits the maximum number of peripheral nodes connected simultaneously. In addition, they usually provide passive monitoring functionalities, while VeriMask is designed for automatically verifying the specific conditions required by MH decontamination.

3 OPEN SOURCE DESIGN FOR EMERGENCY DECONTAMINATION

The failure of traditional production methods to meet the massive demand for PPE during the COVID-19 pandemic has led to rapid response from the scientific community on developing new technologies and tools for emergency use. In particular, Free and Open Source Hardware (FOSH) has been recognized as beneficial in emergency situations due to its high accessibility and the collective contributions from worldwide expertise which enables fast development [75, 81]. VeriMask is the first realization of open source design for safe verification of moist-heat decontamination that is fully integrated with clinical workflows, and was broadly shared with a volunteer collective [89](registered 501(c)(3) non-profit) of scientists, engineers, clinicians, and students from universities and health systems across the world and professionals in the private sector. In this section, we describe the design criteria, challenges, and specifications we formulated developing VeriMask based on our experience and interaction with stakeholders in this collective.

3.1 Foundational Design Criteria & Guidelines

Leveraging the design experience and critical implementation factors highlighted by previous FOSH works and open source medical hardware design [36, 47, 62, 76, 91, 96], we have formulated the following 3 foundational criteria and corresponding guidelines for designing VeriMask. These criterion and guidelines are, in many ways, generally applicable to emergency response hardware design.

Criterion 1: Fast design & deployment. The emergency caused by shortages poses severe risks of infection to health workers due to the prolonged use and reuse of PPE while treating sick patients. A timely design and deployment for protection thus become crucial [53, 84]. Designing simple and highly debuggable open hardware devices significantly accelerates the implementation, deployment, and maintenance processes [47, 76], and helps build a trustworthy relationship between designers and healthcare facilities [47]. In addition, utilizing common off-the-shelf (CoTS) components built and tested by trustworthy manufacturers and available in bulk facilitates implementation and enhances hardware reliability by avoiding long-time testing, calibration, and availability problems due to custom hardware. Unlike devices with novel sensing functionality or materials, it is imperative that emergency response open source design use "boring" but reliable devices to ensure real-world use.

Criterion 2: Generality-oriented robust design. The desired generality is two-fold. First, the function-specific design should be made applicable to a large scope of deployment scenarios, e.g., using various types of heating devices. The actual use case of the design in hospitals is usually unpredictable because of the variance in the existing equipment that different healthcare facilities already posses. In addition, the designers often do not have direct access to the deployment environment due to healthcare regulations [53, 54], which further undermines the feasibility of a dedicated design. It is thus crucial in the design process to assume a weak dependence on the deployment environment and relevant equipment so that it can be easily and widely adopted by different entities for the target purpose. Second, the building blocks of the open source design should have general and common enough functionality plus interface. The design should be able to integrate well with existing infrastructures. For instance, employing popular communication schemes such as WiFi, Bluetooth, and USB not only reduces the cost of the system by eliminating DIY communication modules, but also enables easier development, debugging, replacement, and use. Ensuring such general and common interface enables the designers to easily replace the components in case of a local supply-chain shortage. Generally speaking, ensuring a generality-oriented design also helps make the open source design transferable and reusable for future systems, and makes parts obsolescence (common in the electronics industry) less likely.

Criterion 3: Priority-centered design. The most important criterion for making such healthcare-related open source design is to enforce a priority-centered principle in the specification formulation process. To achieve that, we propose 3 categories of design goals ordered according to their priorities. 1) Safety. Safety requirements

are those that can directly endanger the operators and/or intended users if not met. For example, being able to accurately and reliably determine whether each mask has been successfully decontaminated or not is a safety requirement for our mask decontamination system design. Safety requirements are the most important and must be satisfied before other specifications can be considered [23, 36, 91]. To ensure safety, the designers should fully understand the standards and requirements in government regulations and academic publications, choose the sensor monitoring scheme based on the worst-case scenarios, and carefully evaluate the information loss and consequences in sensor data transmissions. 2) Effectiveness. We define effectiveness as a combination of the degree of achievement for criterion 1 and 2, as well as other performance factors such as designed system's throughput, cost, battery life, and size (in the case where portable devices are desired). Considering the large number of form factors, the designers should develop rubrics for prioritizing the factors and understanding performance. Besides ensuring safety and fast development of VeriMask, we determine scalability, low-cost, and small-size as the top-3 factors to make sure under-resourced hospitals can quickly deploy the platform in large scale. 3) Usability. Usability includes factors such as reducing the workload of the users, making the design easy to use and understand for non-expert operators, and making the devices more comfortable to use (especially in the case of wearable devices). Designers should always design with the clinical operating protocol in mind for improving the actual usability. To ensure high usability of VeriMask, we target at automating the process of mask decontamination verification, maximizing the decontamination throughput, and minimizing the workload of configuring and maintaining the VeriMask platform. In general, these priority mappings hold across emergency response design, as safety, effectiveness, and usability can serve as a rubric for evaluating possible solutions.

3.2 Challenges of MH Decontamination

The most effective methodology of moist-heat decontamination that has been validated on different N95 mask models consist of treating the contaminated masks by holding them within a target temperature range T_l<T<T_h (usually 70-85°C) and relative humidity range RH_l<RH<RH_h (usually 50-100%) for a certain period of time t_{decon} (typically 30-60 minutes) [39, 48]. Higher temperatures can damage the masks filtration capacity, sealing, and fit, while a temperature and relative humidity below the target range or a reduced decontamination time cannot ensure an adequate bioburden reduction. While these requirements might appear relatively simple, there are several challenges in designing a verification platform for decontamination, particularly because the characteristics of MH decontamination processes introduce additional safety and reliability requirements qualitatively different from those in general-purpose monitoring devices.

Handling N95 masks. N95 masks, which can be subjected to the decontamination process for up to five times (cycles) [18], should avoid compression during decontamination that could compromise the sealing and fit characteristics. In addition, cross-contamination between masks should be avoided because bacteria from the user can remain trapped on the mask surface and survive the treatment. MH decontamination processes are indeed intended only for virus inactivation, not for complete N95 masks sterilization [39]. For these reasons, the N95 masks must be kept physically separated (see Figure 1, Phase 1) and returned to the original user after decontamination. Generally, this requires holding each mask in separate sealed rigid containers with a specific amount of water solution to help maintain the moisture environment and labeling each mask with the user data [17]. Thus, the main challenge consists in designing a monitoring platform that can verify the target temperature, humidity, and decontamination time for each mask in isolated micro-environments over multiple heating cycles and integrating it with the healthcare guidelines.

Human Factors. The logistics guidelines of implementing clinical decontamination require trained operators (e.g. healthcare workers or technicians) assigned to the decontamination process [14], who are responsible for maintaining adequate hygiene workflow and manually inspecting each N95 mask before it can be returned to the original user. Typically, the manual inspection consists of discarding masks that are visibly damaged or

have exceeded the maximal allowed number of decontamination cycles. Since the inspection is only based on visual characteristics, the operator is unable to determine if the decontamination has been unsuccessful (e.g. with temperature or humidity drop) so the masks are still contaminated. An effective verification tool needs to address the challenge of enabling the operators to conduct accurate and fast verification by providing reliable feedback.

Non-specialized Commercial Devices and Unpredictable Failures. One major advantage of MH decontamination is its use of commercial heating devices equipped by hospitals which are considered suitable for emergency decontamination [17]. However, such non-specialized heating devices inherently suffer from the problem of non-uniform heat distribution as well as complex and uncontrolled heating dynamics [45, 78, 80, 102]. For example, considering the total MH process time t_{MH} as the sum of the transient time and decontamination time, i.e., $t_{MH} = t_s + t_{decon}$, we found with a clinical humidity chamber more than 20 minutes of transient time variation for reaching the decontamination temperature in different zones (Figure 2 (a)), and more than 9 degrees of difference between the device's set temperature and the internal temperature of the containers even when the cabin was pre-heated (Figure 2 (b)). Such heating dynamics are also affected by the load and initial temperature conditions. In addition, unpredictable failures such as humidity leakage can also happen due to operational errors during the treatment. These challenges make a static preventive device profiling using conventional thermal profilers [33] insufficient and call for real-time verification technologies. We discuss these factors in Section 6.

Throughput Optimization. Another challenge of deploying efficient MH decontamination processes is achieving optimal decontamination throughput, i.e., ensuring the maximum number of successfully decontaminated masks in given time. Ideally, this could be achieved by a full control of the heating device to dynamically adjust the temperature and ventilation of the cabin. However, the large variations in heating devices hardware and software as well as the impracticality of a nurse or healthcare worker modifying/customizing commercial heating devices make it infeasible to realize such a closed-loop control while maintaining wide applicability, fast & reproducible design, and low cost. For these reasons, solving the challenge requires developing a reliable method for predicting the decontamination throughput and providing the user with the optimal settings that achieve throughput maximization without being specific to a particular heating device.

3.3 MH Decontamination Process Integrated with VeriMask.

We designed a clinical workflow, with input from the volunteer collective, that would be as low burden as possible using VeriMask. As shown in Figure 1, the typical operating procedures of a MH decontamination cycle with VeriMask can be broken down to three main phases [17]. During phase 1, the operator preheats the heating device to the target temperature (~80°C) based on the adopted MH treatment, and configures the VeriMask smartphone app with the appropriate thresholds for temperature (T_h and T_l), humidity (R_h and R_l), and decontamination time (t_{decon}). Each contaminated N95 mask is then put into a separate rigid container (e.g. polypropylene, or oven safe Pyrex glass) with (a) the VeriMask sensor node attached to the lid to avoid direct contact with the masks, and (b) a paper towel soaked with 500 μL of water (see Figure 4). Then, each container is sealed by properly closing the lids and transferred into the heating system for the treatment. The duration of this phase can take approximately 20-30 minutes depending on the mask batch size. Phase 2 consists of waiting for the predetermined MH process time t_{MH} for one cycle of decontamination. In this delicate phase, VeriMask automatically checks if the critical process conditions are met and declares decontamination failures if certain anomaly conditions happen (e.g., the relative humidity level falls below the lower threshold). This phase can take 40 to 60 minute based on the MH process adopted, masks' model, and heating device used. Finally, in phase 3 the operator removes the containers from the heating device and sorts each mask based on the mask status shown on the VeriMask monitor application. The masks can either be returned safely to the original user, discarded, or reprocessed if necessary based on the clinical policy. This last phase might have a duration of 5-10 minutes depending on the

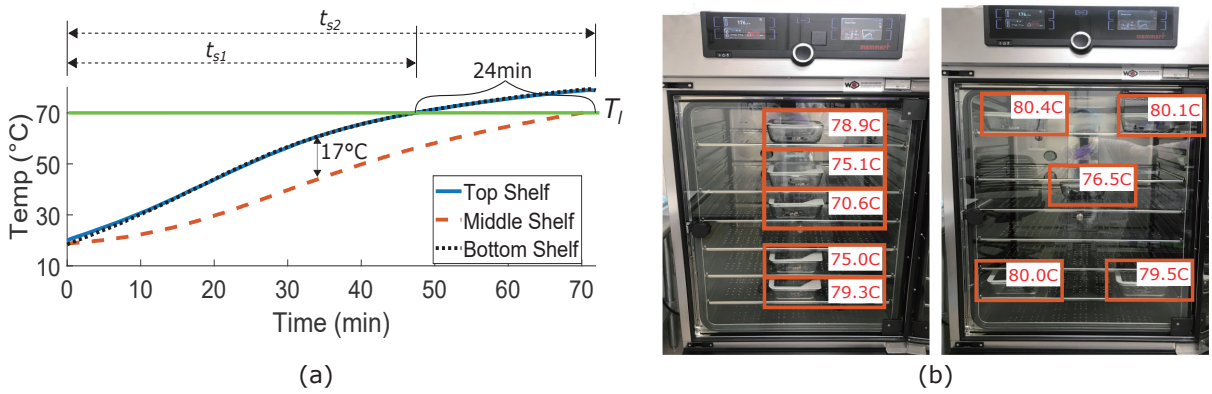

Fig. 2. (a) Temperatures and transient times measured with VeriMask on three different shelves of a clinical humidity chamber during the heating process (starting from 19°C room temperature). The middle shelf container reaches the target temperature of 70°C 24 minutes after the containers on the top and bottom shelves. (b) The 10 locations chosen to measure the non-uniform heat distribution in the pre-heated clinical humidity chamber. The temperature values (in red) show more than 9 degrees of difference in the internal temperature of the containers even 30 minutes after the cabin reached the target temperature (82°C) measured by the heating device built-in sensor.

mask batch size. Once each cycle is ended, the sensor nodes can be reset in the app, and then the containers can be filled again with a new batch of masks to decontaminate in the next cycle.

Profiling cycle. Every cycle monitored via VeriMask can be used as a profiling cycle. When this functionality is enabled using the application, the operator can input the expected total working time defined as the continuous decontamination time in a day (e.g. 8 hours). The temperature and humidity information collected during this profiling cycle (with a default process time of $t_{MH} = 50min$) are then used to compute the optimal heating device temperature and process time for achieving the maximum number of decontaminated masks in the selected working time. The application also provides information about container locations not suitable for decontamination so that operators can avoid placing masks in these areas. If the operator confirms the optimization parameters, the process time for following decontamination cycles are automatically adjusted.

4 VERIMASK DESIGN

Figure 3 shows the architecture of the VeriMask platform. The platform consists of two major components: wireless sensor nodes and an application running on smartphones. The nodes, each one associated with an N95 mask, periodically send temperature and humidity data to the application which performs real-time monitoring, verification of the decontamination conditions, and optimization of the overall decontamination process.

4.1 VeriMask Sensor Node

We designed and manufactured the VeriMask sensor node V1 for experimental testing and performance evaluation, and node V2 for practical clinical usage and deployment. The two versions of sensor nodes are shown in Figure 4.

The VeriMask sensor nodes have been designed to resist the harsh environmental condition of repeated heating cycles by selecting components and making the optimal layout to be high temperature resistant. Each sensor node consists of a Laird653 wireless module with a Nordic nRF52833 SoC [7] that features a maximum operating temperature of 105°C which is suitable for the MH decontamination requirements. It is powered by a

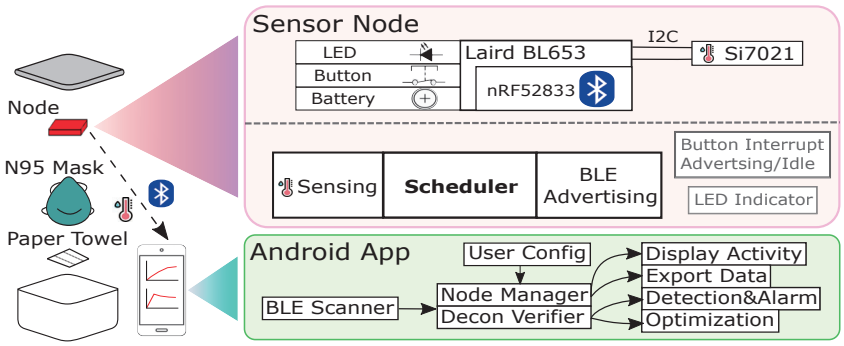

Fig. 3. VeriMask Architecture. The VeriMask platform consists of BLE sensor nodes acting as peripheral data collectors, and an Android application acting as the central monitor and verifier.

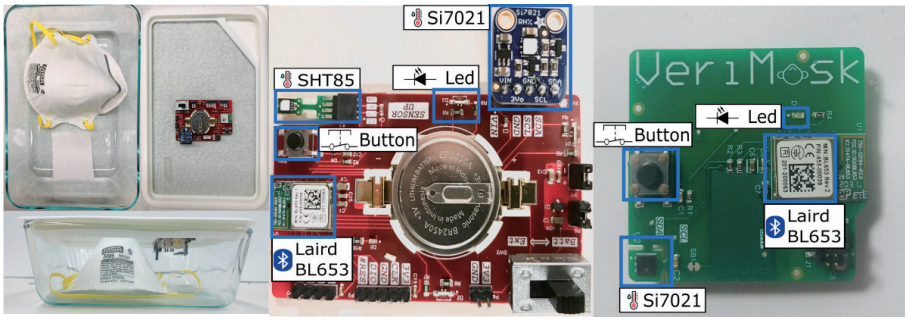

Fig. 4. (Left): The prototype VeriMask V1 sensor node attached to the lid of the Pyrex container along with the N95 mask and the paper towel. (Middle): VeriMask V1 sensor node. (Right): VeriMask V2 sensor node.

high-temperature (125°C maximum), lithium poly-carbonmonofluoride coin cell battery with 550 mAh capacity (Panasonic BR2450A).

The sensor node V1 board includes sockets for two temperature and relative humidity sensors' breakout boards, namely the Adafruit Si7021 containing Silicon Labs' Si7021-A20 sensor [4], and the Sensirion SHT8 containing Sensirion's SHT35-DIS sensor [5], to facilitate testing and replacement of the sensors. The sensor nodes also include a user button to stop and restart the data transmission as well as an LED which blinks while collecting and transmitting data as an extra indicator for the operators. We then label each node with its nodeID on the back which corresponds to the nodeID in its BLE broadcasting packets, and attached the nodes on the lids of the containers to avoid contact with the masks, and with their back side facing upward so that the operators can easily see the nodeID through the transparent lids as shows in Figure 4. Sensor node V2 was designed with the design goals of low cost, simplicity, reliability, and manufacturability. We greatly reduced the number of components, brought down the board to two layers, and reduced the size by more than half, measuring only 3.5cm x 3.8cm (1.4 inches x 1.5 inches). As a result the cost was reduced from $38.27 per board (V1) to $15.66 including components, manufacture, and assembly from a U.S. based manufacturer at a quantity of 1000.

The number of sensor nodes. VeriMask uses a dense one-for-one topology by associating one sensor node to each individual mask. The choice of this topology compared to others (e.g. one-for-many [69]) depends on two main factors. First, using a single sensor to monitor a group of masks requires that the heat and humidity gradients in the sensor node area should be small and should not be subjected to significant variations. However, as shown

in previous work [45, 78, 80] and Figure 2, it is strongly dependent on the heating device characteristics and the MH decontamination process. Thus, the number of sensors nodes used should vary based on a careful thermal and humidity profiling of every heating device as well as every state of the decontamination procedure beforehand. This prevents the rapid deployment of the decontamination technology and makes it impractical, burdensome, and error-prone for non-specialized operators. The second factor is the use of separate sealed containers for each mask. The individual containers are used in MH decontamination processes to avoid cross-contamination between masks and shape deformation, and also to provide the adequate humidity environment for an effective decontamination. Temperature and humidity fluctuations (e.g. leakage) in sealed containers are extremely difficult to measure from outside the containers and might lead to undetected decontamination failures.

Sensor selection. The temperature and relative humidity sensor is a crucial component of the VeriMask platform. The sensor should be chosen based on its reliability to accurately detect changes in the environmental conditions during decontamination, its cost, and its power consumption. Figure 5 (a) shows the critical parameters of four potentially suitable sensors designed to operate under high temperatures (125°C maximum) [2, 4, 5]. We consider the sleep currents as the most important parameter for identifying power consumption of the sensors because for MH decontamination monitoring scenarios the temperature and relative humidity change slowly over time (and the required sample rate is extremely low), thus the sensor would be in sleep mode for most of the time.

	Cost	Sleep Crt.	RH Prec.	Temp. Prec.	RH Resp.	Temp. Resp.
Si7021-A20	$2.98	0.06μA	±3%	±0.4°C	17s	5s
HIH8130-021	$4.36	0.6μA	±2%	±0.5°C	6s	27s
SHT31-DIS	$3.07	0.2μA	±2%	±0.2°C	8s	>2s
SHT35-DIS	$4.41	0.2μA	±1.5%	±0.1°C	8s	>2s

(a)

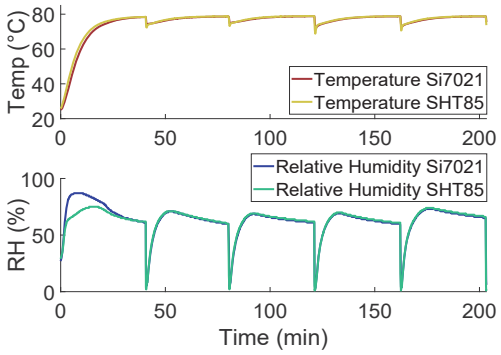

(b)

Fig. 5. (a) Cost, sleep current (Sleep Crt.), relative humidity/temperature precisions (RH/Temp. Prec.) and relative humidity/temperature response time (RH/Temp. Resp.) of 4 high-temperature resistant sensors. We identify the sensor Si7021-A20 as the most suitable for our VeriMask platform. (b) The temperature and relative humidity readings of Si7021-A20 sensor and the SHT35-DIS sensor in 5 consecutive heating cycles.

To find the most suitable sensor for VeriMask, we conducted comparative experiments with the sensor Si7021-A20, which has the lowest cost and power consumption, and the sensor SHT35-DIS, which has the best response times and precision. We used the Sun Electronics EC12 thermal chamber as the convection heating device, and set the time for each decontamination cycle (t_{MH}) to 40 minutes. We did not preheat the thermal chamber so the first heating cycle of Figure 5 (b) shows how the sensors behave when no preheating is performed before decontamination. We use two VeriMask sensor nodes in the chamber, each with one Adafruit Si7021 and one Sensirion SHT85 breakout board (see Figure 4), and perform five consecutive cycles in order to examine the long-term reliability of these sensors.

Experiment results. Figure 5 (b) illustrates the averaged readings of the two VeriMask nodes during the 5-cycle experiment. In the first heating cycle, the maximum and average (absolute) differences in the two sensors' temperature are 4.8°C and 1.8°C, and those in the relative humidity are 22% and 6.8%, respectively. However,

during the following cycles, the numbers decrease to 1.8°C and 0.2°C for temperature differences, and 3% and 0.8% for relative humidity. The differences of readings between the two sensors are generally negligible except for the first cycle, where Si7021-A20 measured a relative humidity overshoot at the beginning, and reported lower temperatures than the SHT35-DIS sensor. The possible cause is that Si7021-A20 has slower temperature response time, and the lower temperature resulted in a higher relative humidity [51]. However, the two sensors had comparable performance in the following cycles, suggesting the Si7021-A20 sensor with slower response time and lower precision is suitable for the MH decontamination monitoring. In addition, using the sensor Si7021-A20 for VeriMask helps to optimize for power consumption and costs. We thus decided to only use Si7021-A20 for VeriMask sensor node V2. All experiments in the evaluation sections are conducted with Si7021-A20 only.

Considerations for decontamination. Another key finding from the above experiment is that without pre-heating the heating system with the containers, the transient time t_s will generally be significantly longer. This could result in insufficient decontamination if the process time t_{MH} is configured to be the same as in a preheated system. To take Figure 5 (b) as an example, while the 40 minute decontamination cycles is enough to keep the N95 masks in the expected decontamination ranges for over 30 minutes with a lower decontamination temperature threshold (T_l) of 70°C, it is not sufficient for the first cycle. The appropriate time for the first decontamination cycle also depends on the specific heating system's heat rate and temperature as well as the expected temperature range. Configuring a separate decontamination period for the first cycle is thus non-trivial. As a result, we recommend to preheat the device to the decontamination temperature before the decontamination starts. We will further discuss the potential failures without preheating in Section 6.

4.2 BLE Communication

The sensor nodes use non-connectable BLE advertising to broadcast sensor data to the Android monitor application. Opting for wireless sensor nodes makes the system flexible and easier to maintain by eliminating the need of wiring for each (potentially hundreds of) sensor nodes. We choose non-connectable BLE advertising over other active BLE modes and synchronous wireless communication methods (e.g. WiFi) for two main reasons. First, these communication schemes limit the number of peripherals that can communicate with the central simultaneously, and increase the power consumption of the sensor nodes as well as the time for adding new nodes into the system [49, 85]. These factors significantly reduce the effectiveness of the platform. Second, custom wireless protocols are generally less supported by commercial mobile devices compared to BLE broadcasting, which is the most common protocol used in smartphones. In Section 5.2 we further demonstrate that with the information redundancy and the low probability of critical information loss, the benefit of having active control is negligible.

BLE broadcasting implementation. The manufacturer-specific data field of the advertising payload contains node identification numbers (nodeIDs) and sensor data. Out of the 31-byte payload space of the non-connectable BLE advertising packet, we use 12 bytes in total with 1-byte nodeID and 4-byte sensor data. The 1-byte nodeID field supports simultaneous decontamination verification of up to 256 N95 masks in a local sensor network. The number can be further increased by utilizing the remaining 19-byte payload space. The sensor nodes broadcast with a transmission power level of 0 dBm to balance power consumption and transmission success rate.

Figure 6 (a) shows the BLE advertising scheme of VeriMask. Each node advertises with advertising interval $t_a = 10s$ by default, which is the time between two consecutive advertising events. The 10s interval is determined empirically based on preliminary experiments' results that temperature and RH have a extremely slow change rate during the decontamination process, and the fact that BLE advertising supports a largest advertising interval of 10.24s. For each advertising event, the node sends three advertising packets on three different frequency channels (channel 37, 38, 39) [82]. Loss of packets can happen due to packet collisions (e.g. packet overlapping in time) on the same channel between different nodes in multi-node scenarios. A 0-10 ms random delay is added before every advertising event in order to mitigate collisions, as is specified in the BLE protocol [6]. If too many

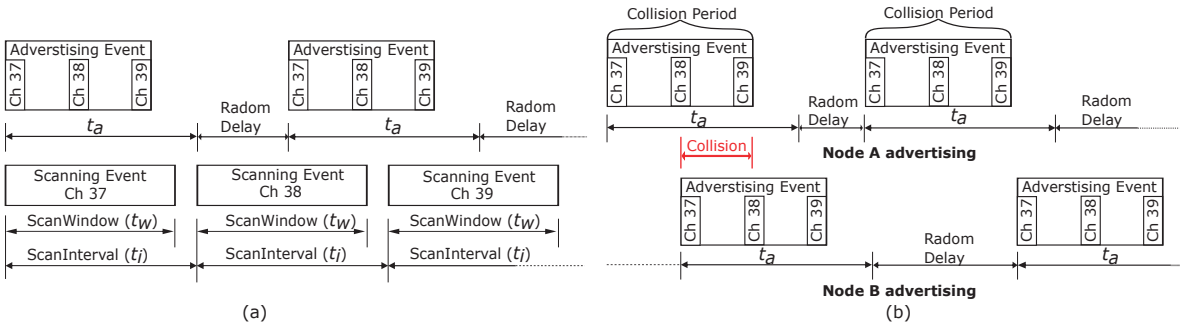

Fig. 6. (a) BLE advertising and scanning scheme (not up to scale) of the VeriMask platform. (b) Advertising collision defined in the multi-node packet collision simulation. If any two nodes' advertising events overlap, a collision happens.

nodes reside in the same local network, however, packet collisions might still happened even with the added random delay. The relationship between packet collision rates and number of nodes in the system thus become an important factor which can affect the VeriMask platform performance. Previous research works [82, 97] have demonstrated the acceptable packet collision rates in dense BLE advertising applications. We further show in Section 5.2 that our BLE advertising configurations guarantee low collision rates and reliable BLE transmission.

4.3 Android Monitoring Application

We choose smartphones as the front-end monitoring device over PCs due to their compactness and pervasiveness. In order to monitor, verify, automate, and optimize the decontamination process of each mask, we built an Android monitoring application prototype. The monitor application's back-end comprises of functional blocks of BLE Scanner, Node Manager, and Decontamination Verifier.

BLE Scanner. We implement the BLE scanner with the standard Android Bluetooth library [8]. In BLE scanning, each scanning event lasts for the period of ScanWindow (t_w) with an interval of ScanInterval (t_i) between each scanning event. t_w should be less than or equal to t_i, with an upper bound of 10.24s for both parameters. The ratio of t_w and t_i is the scanning duty cycle. Figure 6 (a) shows the scanning scheme (not to scale). We configure the monitor smartphones to be in the low-latency scan mode which provides the highest scanning duty cycle [9]. However, it is worth noting that the actual duty cycle also depends on the firmware implementation of different manufactures. As a result, the model of the smartphone can also have an effect on the scanning behavior. We evaluate the performance of BLE scanner with different models of smartphones in Section 5.2.

Node Manager. It is responsible for keeping track of the status of all nodes and the application itself. The monitor application can be in one of the 3 states: IDLE, NODE_DISCOVER (adding nodes into the system), and RECORDING (logging and verifying decontamination process). Based on its decontamination status, each node can be in one of the 5 states: READY (ready for a new cycle of decontamination), DECON (decontamination in progress), ERROR_FAILURE (e.g., temperature/RH does not reach the lower threshold after decontamination starts, exceeds the upper threshold, or falls below the lower threshold, etc.), ERROR_LOST (e.g. the application does not receive the node's packets), and DONE (decontamination completed for this node). State transitions are strictly controlled by finite state machine models as shown in Figure 7 (a).

Decontamination Verifier. The verifier takes the user configuration inputs of the target decontamination ranges for temperature (T_h, T_l) and relative humidity (R_h, R_l) as well as the decontamination time (t_{decon}) within these ranges, and compare them with the sensor reading data. If verification events (e.g., violations of decontamination

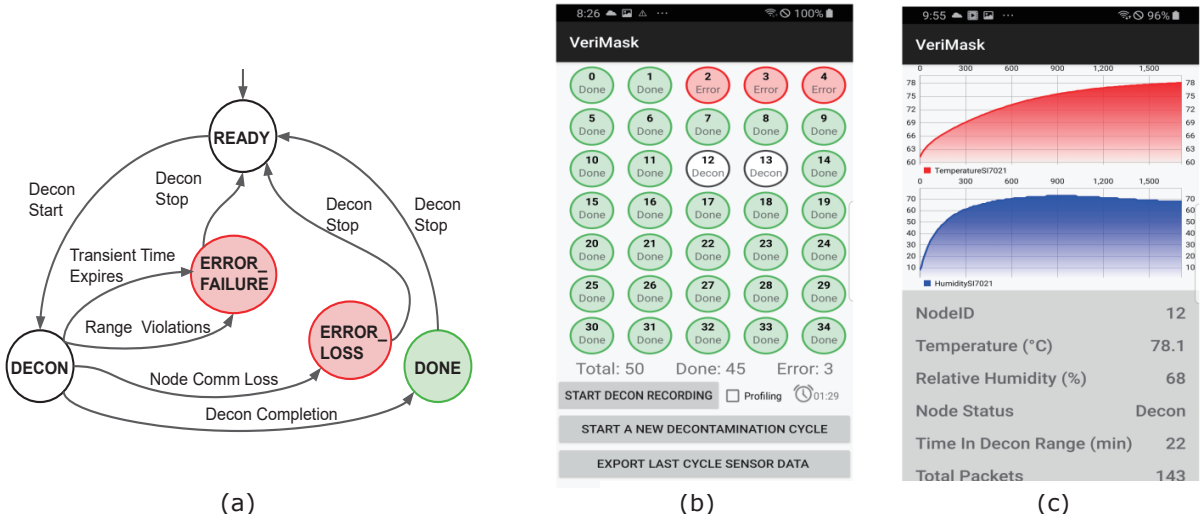

Fig. 7. (a) The sensor node states and transitions in VeriMask Android monitor application. (b) The main control page which shows the states of each individual mask inside the containers. (c) The detail page which displays the information of the sensor node associated with the mask chosen on the main page.

ranges) are detected for a certain node, the verifier reports back to Node Manager which will then change the state of that node. The criteria of verification events and state transitions shown in Figure 7 (a), are as follows.
1) Loss of nodes: If the application misses packets from a sensor node for more than a grace period of 2 minutes continuously, the node state is changed to ERROR_LOST.
2) Decontamination Failure. Three main events can cause violations and a change of state to ERROR_FAILURE: i) when temperature and/or the humidity level of the node does not reach the pre-configured ranges for a grace period of 20 minutes continuously from the beginning of the MH process time t_{MH} (including the transient time t_s), ii) when temperature and/or the humidity level falls out of of the pre-configured ranges for a grace period of 2 minutes continuously after the transient time, and iii) when the node has not completed the decontamination time t_{decon} at the end of the MH process time.
3) Decontamination completion: If the temperature and humidity level have been within the pre-configured range for the decontamination time t_s, the node state is changed to DONE.
Note that the time for the grace periods are the default values, which can be changed by the operator if needed.

User Interface. The user interface consists of three pages, namely i) a main control page and ii) a node details page which are shown in Figure 7, and iii) a decontamination parameter configuration page. The main page lists all the nodes added as well as their statistical information. Operators can check a profiling checkbox and enter profiling mode before each decontamination cycle for throughput maximization (Section 4.4). It also displays a timer count down for t_{MH} which will be determined by throughput-maximization algorithm. When selecting a node, the application navigates to the node details page, where the most recent temperature and relative humidity readings and other node information including node states are displayed. All pages are updated in real time.

4.4 Throughput Maximization

Beside providing monitoring capability, VeriMask has been designed to provide feedback information to help the operators achieve the optimal decontamination throughput, i.e., achieving the maximum number of successfully

decontaminated masks in a given time, based on the heating device used. To build this functionality, we develop a throughput-maximization algorithm for the App that can be used in the profiling phase of the decontamination to determine and suggest the optimal combination of decontamination parameters.

Problem Formulation. The general idea of throughput-maximization is that given a total continuous working time selected by the operators, e.g., 8 hours, and the decontamination data of 1 profiling cycle, the algorithm predicts the heating device temperature and MH process time (t_{MH}) that will generate the highest number of successfully decontaminated masks in the 8 hours. The reason for maximizing the throughput in the total working time instead of just one decontamination cycle can be easily illustrated with an extreme example: decontaminating 19 masks in 30 minutes per cycle is better than decontaminating 20 masks in 60 minutes. The algorithm is based on the assumption of similar dynamics of the profiling cycle with the following decontamination cycles after 1 preheating cycle, as verified in our experiments (e.g., the last 4 cycles shown in Figure 5).

We start by looking at the general optimization problem, where no profiling or other data is given. We denote the selected total working time as t_{work}, the time for the conducted profiling cycle as t_{prof}, the heating device temperature as T_{dev}, the total number of successfully decontaminated masks in t_{work} as n_{work}, and that of each decontamination cycle as n_{MH}. We then have the following equations:

$$\begin{cases} n_{work} = \frac{t_{work}}{t_{MH}} \times n_{MH} \\ n_{MH} = f(t_{MH}, T_{dev}), \end{cases}$$

where $f(\cdot)$ is an unknown deterministic function with parameters such as the heating device model (its heat transfer and distribution functions), container placements, etc. We can now formulate the general throughput-maximization problem as the 2-D optimization problem:

$$t_{MH}^{optim}, T_{dev}^{optim} = \underset{t_{MH},\, T_{dev}}{\text{argmax}}\ n_{work}$$

Note that it is almost impossible to get a closed-form analytical solution because of the unknown $f(\cdot)$. With the data from the profiling cycle and the assumption that each cycles have almost identical dynamics, however, we can instead implement discrete algorithm to search for an optimized numerical solution in a simplified context.

Implementation. Intuitively, by utilizing the profiling cycle's data we can convert the optimization problem into a discrete 2-D search problem for a global maximum. Furthermore, we observe through experiments that the temperature instead of relative humidity of the masks is the limiting factor of transient time t_s in the normal case. For example, the blue stars in Figure 12 that represent the time instance when a mask enter the DECON status are determined by the temperatures. As a result, we only need to consider the temperature data of the masks in the profiling cycle to determine if each mask has been in the decontamination range.

Varying t_{MH} can be easily done on the profiling cycle's data by fixing the start of t_{MH} at time 0 while changing the cycle end time. Varying T_{dev}, however, is more tricky since we only have the data for 1 profiling cycle where the heating device temperature was fixed to a certain value $T_{dev}^{(0)}$. To sweep through different T_{dev} while avoiding increasing the number of required profiling cycles, we use a stretching method that adapts the temperature data of each mask collected in the profiling cycle to temperature curve estimations under different T_{dev}. Based on the observation that changes in T_{dev} does not change the overall trend (the type of underlying time function) of the temperature data curves, we stretch the curves proportionally according to $T_{dev}/T_{dev}^{(0)}$. After that, we can finally apply the optimization (search) algorithm to find the best set of T_{dev}^{optim} and t_{MH}^{optim}. We summarize the algorithm for the above throughput-maximization in Algorithm 1. In the App implementation, $\underline{T}_{dev} = [T_l : 1°C : 100°C]$, $\underline{t}_{MH} = [t_{decon} : 1min : t_{prof}]$, where the 2nd element of each vector represents the discrete step size. After the profiling cycle, the App runs the throughput-maximization algorithm and reports the optimal decontamination parameters T_{dev}^{optim} and t_{MH}^{optim} as well as the expected number

Algorithm 1: Throughput Maximization

Input: selected total working time t_{work}, profiling cycle temperature data matrix D_{prof}, profiling cycle heating device temperature $T_{dev}^{(0)}$, required in-range decon time t_{decon}, decon temperature thresholds $[T_l, T_h]$, optimal heating device temperature (candidate) vector $\underline{T}_{dev}$ and MH process time (candidate) vector $\underline{t}_{MH}$

Output: $t_{MH}^{optim}, T_{dev}^{optim}, n_{work}^{optim}$

Initialization: $t_{MH}^{optim} \leftarrow 0, T_{dev}^{optim} \leftarrow 0, n_{work}^{optim} \leftarrow 0$
for *each candidate* T_{dev} **do**
  $D_{stretched} = stretchTemps(D_{prof}, T_{dev}^{(0)}, T_{dev})$
  for *each candidate* t_{MH} **do**
    $n_{work} = countTotalSuccessfulMasks(t_{work}, D_{stretched}, t_{MH}, [T_l, T_h])$
    if $n_{work} > n_{work}^{optim}$ **then**
      $n_{work}^{optim} = n_{work},\ t_{MH}^{optim} = t_{MH},\ T_{dev}^{optim} = T_{dev}$
    else
      Do Nothing
    end if
  end for
end for
return $t_{MH}^{optim}, T_{dev}^{optim}, n_{work}^{optim}$

of successfully decontaminated masks n_{work}^{optim} using these parameters. The App will also inform the operators of the container locations where the masks are predicted to experience decontamination failures so that the operators can avoid placing masks there. We will further show a case study for evaluating the effectiveness of this throughput-maximization method in Section 5.3.

5 EVALUATION

In this section, we evaluate the performance of VeriMask. We examine the power consumption of the VeriMask sensor nodes in Section 5.1, and examine the reliability of the wireless sensor platform in Section 5.2 by looking into the BLE transmission performance in different scenarios. We conducted these evaluations with two different heating systems, namely a Sun Electronics EC12 thermal chamber in a laboratory setting, and a Memmert HCP humidity chamber in clinical setting. Finally, we analyze the effectiveness of the throughput-maximization functionality in Section 5.3 by carrying out a case study with the EC12 thermal chamber.

5.1 Power Consumption & Battery Life

Circuits' power consumption under higher temperatures increases because of increased leakage current [56]. Due to extreme temperature variation and the high-temperature nature of the decontamination process, we investigate the current consumption and battery life of our VeriMask sensor nodes under different temperatures.

Experimental Setup. The sensor node runs the same program as in the decontamination settings, where the board fires one advertising event every 10s, and one of the LED flashes every 5s for 5ms as an indication of normal operation. The EC12 thermal chamber is used as the heating device. We used an STM32 Power Shield [3] to measure the currents, and configured the supply voltage, sample rate, sample period, minimal current threshold to 3V (same as the supply voltage of the battery), 20000 samples/s, 100s, and 1uA respectively. We left the STM32 Power Shield outside the thermal chamber and used a long jumper wire to connect it to the sensor node to avoid measurement errors of the STM32 Power Shield when undergoing high temperatures. When calculating the estimated battery life, we revise down the total usable battery capacity to a conservative 70% of the specified capacity to account for manufacturing tolerances and other conditions that can degrade battery capacity [52].

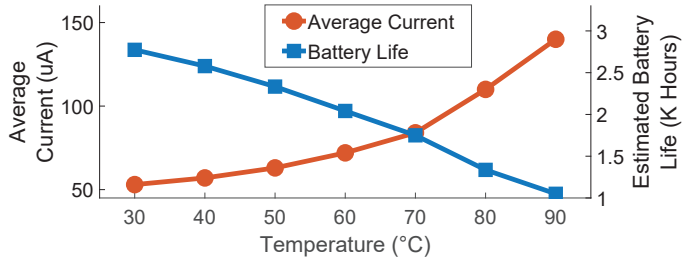

Fig. 8. Average current consumption and estimated battery life (calculated with a conservative 70% of the specified battery capacity) of the VeriMask sensor node under different temperatures. The sensor node is able to work for over 1000 decontamination cycles without changing the battery.

Results. Figure 8 shows the average current and estimated battery life of the VeriMask sensor node under different temperatures. At the highest temperature of 90°C, the estimated battery life is over 1000 hours. Since the nodes temperatures are mostly below this temperature, we can assume our node can successfully monitor continuously for over 1000 hours. Assuming the time needed for decontaminating each batch of masks is 1 hour (20min initial preparation and 40min MH decontamination), our node can support 1000 N95 mask batches without the need of replacing the battery.

5.2 BLE Transmission

Both multi-node packet collision and single node packet loss prevent successful sensor data transmission over BLE in VeriMask. Since our scalable system is designed to support decontamination of up to hundreds of masks simultaneously, packet collisions might cause non-trivial packet losses in a multi-node scenario as pointed out in Section 4.2. In addition, each node's packet transmission will be affected by the condition of the transmission path such as blocking of wireless signals by the glass container and metal chamber, distance between the node and smartphone, etc., as well as by the behavior of the scanning device. As a result, BLE transmission success rate of the system is a function of these two independent factors. We thus consider the them separately in this section.

Multi-node packet collision rate $R_c^{(n)}$. Evaluating multi-node packet collision rate with real hardware nodes is impractical due to the large number of nodes required. We instead conducted software simulations with MATLAB 2019 to calculate the collision rates $R_c^{(n)}$, where n denotes the number of nodes. The advertising configurations are the same as in 4.2. However, we simplified the collision condition introduced in 4.2 (overlapping packets on a certain advertising channel) to the following. If any two nodes' advertising events overlap in time (all three channels considered), we define the two advertising events as having a collision. We thus define the time of each advertising event as the collision period. Figure 6 (b) demonstrates the collision scenario. The simplification will result in higher collision rates than the actual rates since previous non-collision conditions such as node A channel 37's packet overlapping with node B channel 38's packet will now be treated as a collision. Another simplification we made is that we use all 31 bytes in the payload instead of the 12 bytes we actually use, which result in longer collision period for each advertising event and thus higher collision rates. As a result, we claim that our simulation results show a loose upper bound of the actual collision rate.

The advertising interval t_a is set to 10s (default). Based on the information from the Nordic Online Power Profiler [22], we set the collision period to 1.7ms. We then set the simulation resolution (size of the minimal discrete time step) to be 0.1ms. For each number of nodes, we simulated 100 4000-second trials with the advertising start time of each node chosen randomly within the first 10s under a uniform distribution. The mean and standard deviation of the packet collision rates with different number of nodes are calculated and shown in Figure 9. The packet collision rates with 100 nodes is lower than 4%. Our results comply with previous works of BLE advertising

collision rates simulation [82], which suggests a packet collision rate of about 5% with 300 nodes. This result shows that active packet collision avoidance will result in minor performance improvements at the cost of higher power consumption and limitations in the total number of nodes that can be connected simultaneously.

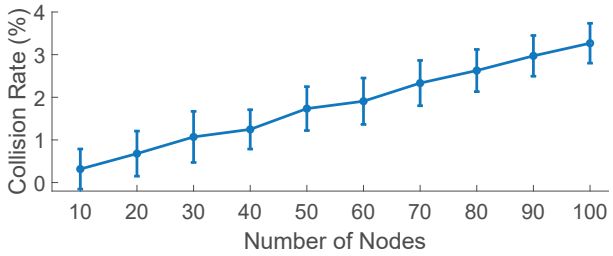

Fig. 9. Packet collision rates per sensor number. The low collision rates suggest that active packet collision avoidance is unnecessary which will negatively affect the nodes' scalability and battery life.

Single-node packet loss rate R_l. The glass container and the metal enclosure of the heating equipment can degrade BLE signal strength along the transmission path. Different scanning behaviors of the scanning smartphones due to differences in hardware and versions of library codes can also affect the possible number of received packets, even if the smartphone is configured at low power scan mode. For example, different firmware implementations might define different BLE scanning duty cycles for the low latency scan mode. It is thus important to know how many packets might be lost due to these effects.

To test the single-node packet loss rate, one glass container holds one sensor node with its lid closed and was put in the closed heating system. We then collect the data using two heating systems, namely the EC12 thermal chamber and the clinical Memmert HCP humidity chamber. A Samsung Galaxy Note4 (Android 6.0.1), a Samsung Galaxy S8 (Android 10), and a Google Pixel2 (Android 9) were used as the monitor smartphones. During the test, the sensor nodes generated one advertising event every 10s as the default setting. We then incremented the distance between the node and the smartphones from 10cm to 150cm with a step size of 20cm. For each distance, the transmission lasts for 400s (40 advertising events in total). Figure 10 (a) shows the measured packet loss rate versus distance to the thermal chamber, and Figure 10 (b) shows the results with the humidity chamber. Generally, there are only small increases in packet loss rates for each smartphone when the distance reaches 1.5m for both heating systems. The measured loss rates in all the selected distances are less than 25%. The seemingly high single-node packet loss rate is due to the poor SNR caused by the metal enclosure of the heating devices, which acts as a Faraday cage. The EC12 thermal chamber has a 25.4cm x 12.7cm (10inches x 5inches) small double-layer glass window on the metal enclosure. The clinical Memmert HCP humidity chamber (shown in Figure 2 (b)) is fully covered by metal when the door is closed (note that Figure 2 shows when the door is open). As a comparison with previous research results, [86] found that metal enclosure can reduce the BLE RSSI by over 15dB. Meanwhile, [58] found that with a distance of 1m and a BLE transceiver power of -12dBm, the BLE open-air broadcasting packet loss rates with smartphones as the centrals are about 20%. Our results show that with 0dBm transceiver power and metal enclosures the packet loss rate is less than 25%, which is consistent with the previous works. It is also worth noting that such packet loss due to the metal enclosure is an issue for not only BLE, but also all other wireless communication schemes [64, 70, 72]. However, we will show that it causes negligible information loss in our application because of the slow change rate of the temperature and humidity.

Overall packet loss rate $R^{(n)}$. Calculating the overall packet loss rate $R^{(n)}$ with n nodes includes combining $R_c^{(n)}$ and R_l. The theoretical value of $R^{(n)}$ can be calculated as $R_l + (1 - R_l) \times R_c^{(n)}$. Based on the experimental results, we get $R^{(100)} = 28\%$ if we consider the worst-case scenario where $R_c^{(100)} = 4\%$ and $R_l = 25\%$. Even considering

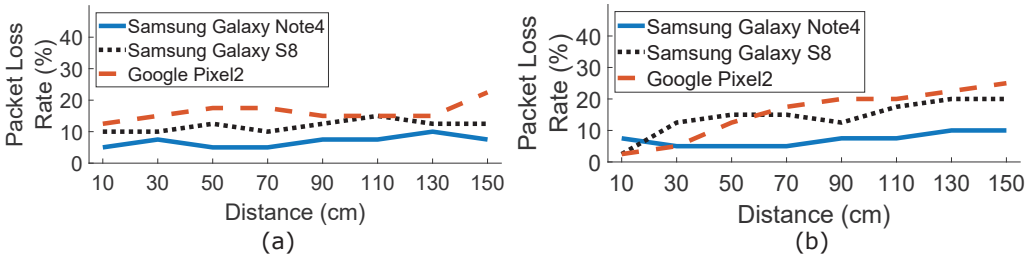

Fig. 10. Single-node packet loss rates at different distances. (a): With the EC12 thermal chamber; (b): With the clinical Memmert HCP humidity chamber. The seemingly high packet loss rate is due to the metal enclosure of the heating devices, which acts as a Faraday cage for RF signals and is thus challenging for all types of wireless communications.

this the upper bound for the overall packet loss rate, it is still small enough to support robust close-distance monitoring. Furthermore, it is worth noting that during the actual MH decontamination process tests where the operating temperature of the nodes rise over 80°C, we didn't observe any increase in overall packet loss rates.

Information Loss. After getting an estimate of the overall packet loss rate's upper bound during decontamination, it is necessary to inspect the degree of information loss and the potential effects on the monitoring capability. To this end, we categorize the loss of data into two classes, namely non-critical and critical data loss. 1) Non-critical data refers to the packets that do not contain temperature and humidity data outside of the desired decontamination range. In another word, it captures the normal temperature and humidity variations. For this class of data, our experiments conclude that the temperature and humidity change rate will generally be smaller than 1°C/30s and 3%/30s respectively. Assuming the overall packet loss rate reaches the upper bound 30%, then the probability of missing a mask's data for 30s is only 2.7%, which is negligible. Furthermore, we can easily recover the 2.7% lost data with techniques such as matrix completion [43, 46] if necessary. This is because the normal temperature and humidity variations for all of the masks are essentially low-rank, i.e., having a large amount of information redundancy. 2) Critical data can be further classified into two sub-classes. The first class results from decontamination failures that affect all masks in the heating device. For instance, if the door of the heating device is accidentally left open, the temperature of all masks will fall below the decontamination lower threshold following the same trend. In this case, the same matrix completion technique can be used since the variations are still low-rank. The second class of critical data results from errors of an individual masks. This class of critical data cannot be easily recovered with the matrix completion technique because the mask's abrupt and abnormal temperature/RH variations don't follow the same trend as the other masks. Luckily, there's actually no need for recovering this class of critical data since such type of single-mask anomalies are mostly caused by operational errors which make the abnormal variations irreversible. We can thus eventually detect this irreversible anomaly even with (unusual) consecutive packet loss. For instance, if a humidity leakage happens in a certain container and causes a mask's relative humidity to fall below the lower threshold, the anomaly is permanent and will be eventually detected even if the 2.7% packet loss happens during the first 30s.

Long-distance Monitoring. The above discussion shows that VeriMask's BLE communication can support reliable close-distance monitoring when the operator with a smartphone is within a range of 1.5m from the sensor node. While this range is the most common for mask decontamination operations [14], the operator may occasionally move outside this range. We thus tested the packet loss rate and signal strength at larger distances in a lab environment with the EC12 thermal chamber. We found that when the distance increased from 1m to 5m, the average packet RSSI reported by the 3 smartphones decreased from -65 to -83 dB while the packet loss rate was lower than 35% for all 3 smartphones. We also tested a through-wall scenario where the smartphones and

sensor node in the chamber were separated by a 15cm wall and 3m away from each other, and found a -81dB RSSI and -32% packet loss rate on average. With an upper bound of 50% for the packet loss rate, we found that the BLE communication could achieve up to 11m in a room, or 7m across rooms with the 15cm wall. All the experiments were conducted with normal radio and human movement interference in the environment. These results show that VeriMask also has the potential to support a relatively long distance monitoring and further enhance usability.

5.3 Throughput-Maximization Case Study

In order to show how the throughput-maximization functionality of VeriMask works and to test its effectiveness, we conducted a case study with the EC12 thermal chamber in a lab environment and 20 VeriMask node-container sets. Figure 11 (a) shows the chamber fully filled with 5 stacks (3 in the back, 2 in the front) of node-container sets with 4 in each stack. We carried out two sets of experiments where in the first one we placed all the 20 node-container sets in the chamber while in the second one we removed the node-container sets on the top of each stack and used only 15 containers and sensor nodes. For each experiment, we first set the temperature of the chamber ($T_{dev}^{(0)}$) to 85°C and ran a 50min (t_{prof}) profiling cycle and then calculated the throughput-maximization parameters ($T_{dev}^{optim}, t_{MH}^{optim}$) and the expected number of successful node-container sets (n_{work}^{optim}) with Algorithm 1 by setting the total working time t_{work} to 50min. Note that here we define "successful" as the event that the temperature of a node-container set remains in the decontamination range for 30min since the humidity is not the limiting factor for throughput as pointed out in Section 4.4. We then set the heating device temperature to T_{dev}^{optim} and ran another decontaminating cycle for t_{MH}^{optim} and inspected the actual successful node-container sets.

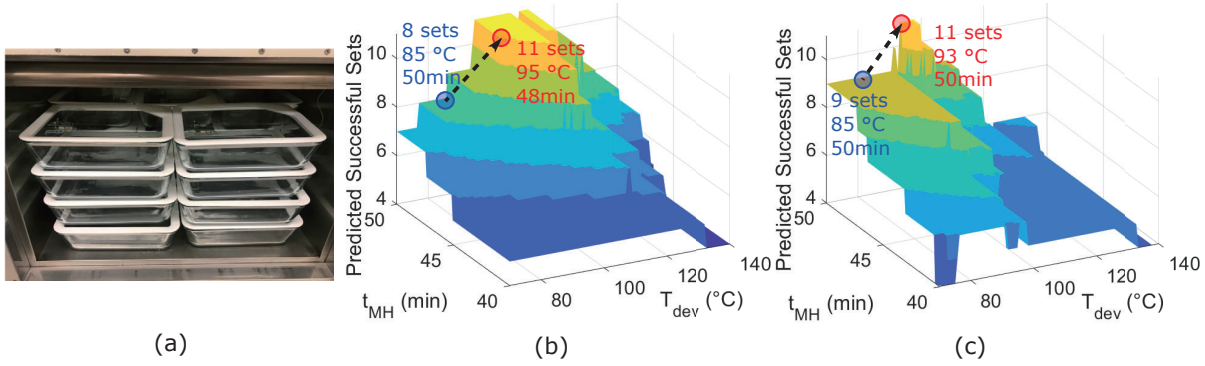

Fig. 11. (a) The EC thermal chamber fully filled with VeriMask sensor nodes. (b) With 20 containers in the chamber for the profiling cycle, the Algorithm 1 predicts that the maximum throughput of successfully decontaminated masks in 50min is 11 out of 20 when $T_{dev} = 95°C$ and $t_{MH} = 48min$. (c) With 15 containers in the chamber for the profiling cycle, the Algorithm 1 predicts that the maximum throughput of successfully decontaminated masks in 50min is 11 out of 15 when $T_{dev} = 93°C$ and $t_{MH} = 50min$. In (b) and (c), the blue circles mark the decontamination parameters used in the profiling cycle,and the red circles mark the optimized decontamination parameters. The arrows show the direction of optimization.

Results. Figure 11 (b) and (c) plot the prediction results of Algorithm 1 for the two experiments with the data from their respective profiling cycles. In the profiling cycles, 8 and 9 sets were found successful respectively in the case of 20 and 15 total node-container sets, as is marked by the blue circles in the figures. The algorithm predicts 11 successful sets in both cases with their respective optimized parameters as marked by the red circles in the figures. It is worth noting that the predicted successful sets in the two cases were different. For example, in the

20-container case all the 5 sets on the top of each stack which were removed later were predicted to be successful, which means some unsuccessful sets in the 20-container case became successful in the 15-container case due to the changed container number, placements, and the resulted change in heat distribution in the chamber.

In the following decontamination cycle using the optimal parameters given by VeriMask, we verified that 11/20 and 12/15 sets were successful respectively, which are highly close to the prediction results (11/20 and 11/15). In addition, there were only 1 mismatch in the predicted and actual successful sets in both cases. The results suggest VeriMask can improve the decontamination throughput in a reliable way.

Key insights. Besides the verification of the throughput-maximization scheme, there have also been some key observations and insights from these 2 sets of experiments. First, using more containers doesn't guarantee more successfully decontaminated masks, as shown by the comparison between the 20-container and 15-container cases. This paradox is caused by the fact that too many containers slow down the convection and thus the heat transfer in the heating device. The EC12 chamber is a convection oven with hot air outlet at the top-front of the chamber. In the 15-container case, we observed more successful node-container sets at the bottom and in the back of the chamber even with lower temperature (93 v.s. 95°C) due to the removal of the 5 top-layer containers blocking the hot air. Figure 11 (b) (c) also implicitly show this effect since the high-temperature area in (c) generally has fewer successful sets than in (b) because with fewer containers and better convection, higher temperatures tend to drive the mask temperatures higher than the upper threshold more easily and thus cause failures. This insight suggests that when there is a large difference between the number of containers used and the predicted successful ones (e.g., 11 v.s. 20), the operators can try removing some containers to get better decontamination throughput and reduce the overall workload. Second, the number and placement of containers are verified to largely affect the heat transfer and distribution in the heating device. This again shows that a simple thermal profiling of the heating device with conventional equipment [33] is not sufficient to ensure reliable decontamination processes thus the necessity of VeriMask for real-time monitoring. Third, decontamination throughput can vary fiercely when using different parameters as shown in Figure 11 (b) (c), so the throughput-maximization feedback scheme realized in VeriMask can effectively guide the operators for setting the optimal parameters.

6 DECONTAMINATION FAILURES ANALYSIS & DETECTION

Detecting failures in the decontamination processes is the key to the reliable verification. In this section, we analyze the factors that can potentially cause decontamination failure, and how VeriMask automatically detects different types of decontamination errors in real-world scenarios.

6.1 Non-uniform Heat Distribution

Non-uniform heat distribution in the heating system causes "hot spots" and "cold spots", that can potentially lead to (i) decontamination failure in case the target temperature is not achieved, or (ii) damage to the mask filtration if the temperature is too high. In order to examine this scenario, we evaluate with VeriMask the heat distribution under different operating conditions.

Experimental Setup. The experiments were conducted with the clinical Memmert HCP humidity chamber. Note that we disabled the humidity generation function to emulate heating systems without humidifying functions.

Dynamic heat distribution. We put three sets of containers and sensor nodes on the top, middle, and bottom shelf of the humidity chamber (set to 82°C) to measure with VeriMask the heating distribution with the system start heating from ambient temperature (19°C). Figure 2 (a) shows the temperature readings of these three sets of containers through the whole process. The graph shows that the maximum temperature variations in these locations is 17°C. The middle shelf has the lowest temperature because it's the farthest from the heating units, i.e., the walls of the chamber. The middle shelf thus requires 24 minutes more transient time (t_{s2}) than the top

and the bottom shelf (t_{s2}) to reach the decontamination temperature lower threshold of 70°C. The results indicate that systems should be pre-heated and given the time to reach a steady-state heat distribution before beginning decontamination cycles. Without a pre-heating step, the temperature variance can be large enough to force a significant increase in the decontamination duration, and certain sections of the oven may become hot enough to overstep the upper temperature threshold, damaging masks within that zone.

Using VeriMask, the operator can conduct a preliminary test with empty containers to simulate the expected cabin load, and thus determine the correct temperature transient time.

Steady-state heat distribution. After the humidity chamber reached the steady state, which we define as 30 minutes after the chamber reached the configured target temperature of 82°C according to the internal temperature sensor of the chamber, we measured with VeriMask the temperatures at 10 different locations (see Figure 2) (b). Among the measured locations, the maximum temperature difference is 9.8°C (between top/bottom shelf and middle shelf). The results indicate that some locations barely reached 70°C when other locations were over 80°C. This suggests that decontamination failures are much more likely to happen to N95 masks put far away from the walls of the humidity chamber. For instance, if the required temperature lower thresholds were higher, the masks on the middle shelf would not be in the target temperature range, causing ineffective decontamination without being detected. Using VeriMask's profiling cycle functionality, the operator can rapidly identify the locations with insufficient heating and respond accordingly. For example, the App can suggest the operator avoid placing masks at these locations in the following cycles, set a higher temperature for the chamber, or set a longer decontamination time.

6.2 Operational Errors

Different operational errors can negatively affect the MH decontamination process. For instance, humidity leakage and insufficient amount of water in the containers are two major factors that can cause decontamination failure. Humidity leakage can arise due to improper sealing of the containers or a manufacturing defect of the heating system or the container. When it happens during decontamination, the relative humidity level of the container often sees a sharp decrease, which can lead to falling below the decontamination humidity range. On the other hand, if the operators wet the paper towel with a smaller amount of water by mistake, the masks will not reach the target humidity range during the decontamination time, leading to decontamination failure. As a result, it is important to examine how VeriMask behaves under these possible conditions.

Experimental Setup. The experiments were conducted with the EC12 thermal chamber and the clinical Memmert HCP humidity chamber (with humidity generation function disable). We set in VeriMask monitor application the expected decontamination temperature range to 70-85°C, the humidity range from 50% to 100%, and the decontamination time t_{decon} to 30 minutes. Each decontamination cycle was 40min, i.e., $t_{MH} = 40min$.

Humidity Leakage. We evaluate the effect of the humidity leakage by comparing the decontamination processes of two sets of containers with the VeriMask sensor nodes. As a baseline, we prepared the first set of containers with the correct amount of water on the paper towel (500uL). For the leakage set, we used the correct amount of water but deliberately created a 1 cm diameter hole in one corner of the lid. Then we ran the decontamination cycle with the EC12 thermal chamber and the Memmert HCP humidity chamber, whose temperatures were set to 80°C and 82°C respectively.

Figure 12 (A2) and (B2) show the relative humidity readings with the two heating systems respectively. The figures also show the time when VeriMask detected the violation of the RH range (in red) and changed the state of the sensor nodes in the monitor application to ERROR_FAILURE (decontamination failure), and when the process is successfully completed (in blue) and changed the state to DONE.

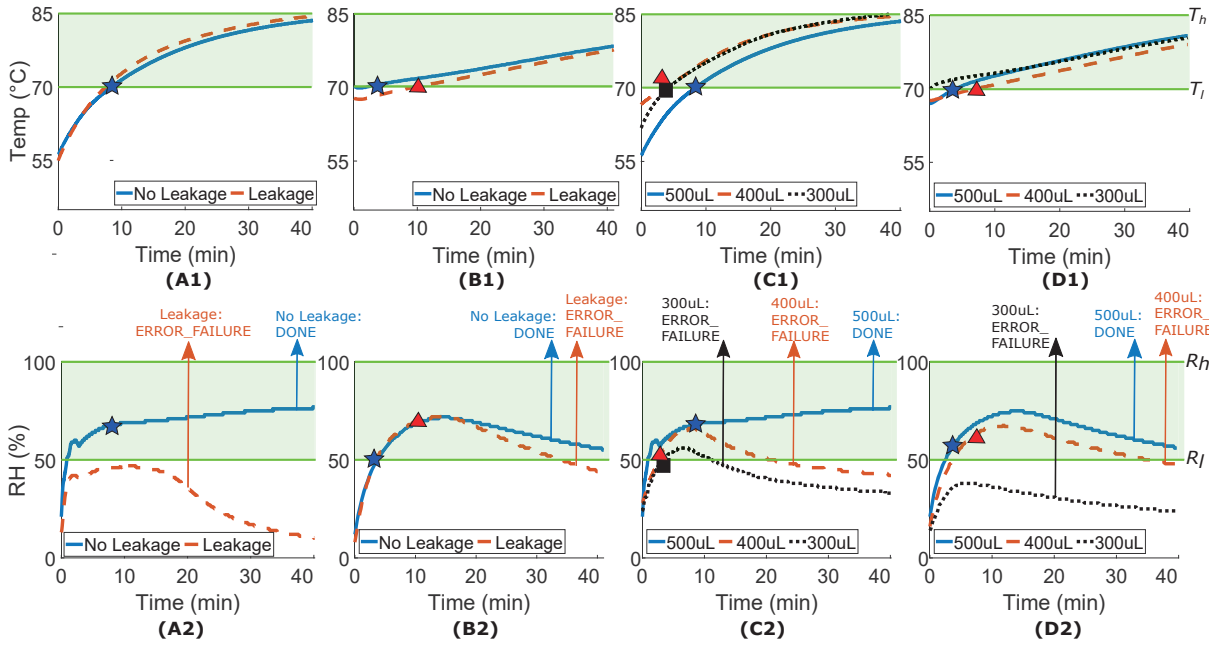

Fig. 12. Temperature, relative humidity, and VeriMask responses during a decontamination cycle where there exist operational errors. (A1) and (A2) show the leakage vs. no-leakage cases with the EC12 thermal chamber in lab setting. (B1) and (B2) show the leakage v.s. no-leakage cases with the Memmert HCP humidity chamber in clinical setting. (C1) and (C2) show the normal (500uL) and less (400uL, 300uL) amounts of water cases with the EC12 thermal chamber. (D1) and (D2) show the normal (500uL) and less (400uL, 300uL) amounts of water cases with the Memmert HCP humidity chamber. The blue star, red triangle, and black rectangular mark the start time when the temperature and humidity readings both enter the pre-configured decontamination ranges (colored in green) for each case.

In the EC12 thermal chamber, the leakage set did not reach the target relative humidity in the decontamination time, which caused a violation event generated by the verifier of the VeriMask application after 20 min as described in Section 4.3. In the clinical humidity chamber instead, the humidity level reached the target range for 28 minutes, then the violation event was generated by VeriMask 2 minutes after the RH level fell below the lower threshold. We argue that this difference is due to the different airflow speeds of the convection heating systems. The EC12 thermal chamber has a higher airflow speed compared to the clinical humidity chamber, which accelerates the convection between the humidified air in the container and the dry air in the heating system, thus rapidly decreasing the RH level.

Insufficient amount of water. We evaluate the effects of using an insufficient amount of water by comparing the decontamination processes of three sets of containers with the VeriMask sensor nodes. The amount of water used for soaking the paper towels was 500uL, 400uL, and 300uL respectively. We then ran a single decontamination cycle with the two heating systems at the same setting as in the leakage experiments.

Figure 12 (C2) and (D2) show the relative humidity readings with the two heating systems, and the change of states of the nodes in the VeriMask monitor application. As shown in the figure, the two sets with 400uL and 300ul both experienced decontamination failure. As in the previous case, if the relative humidity level does not reach the target level during the first 20 minutes, the node changes its status to ERROR_FAILURE.

Overall Observations. From this failure analysis we can conclude that VeriMask can not only help to characterize the suitability of commercially available heating systems to be used as decontamination devices, but also can be easily integrated to standard operating procedure to automatically detect failure conditions that can compromise decontamination processes that might go undetected if rely only on the heating device sensors.

7 DISCUSSION

In this section we consider and discuss feedback from healthcare professionals (Section 7.1) and lay out the lessons learned from our experience and collaboration with the consortium of experts and clinicians attempting to solve N95 decontamination problems (Section 7.2).

7.1 Feedback From Healthcare Professional and Decontamination Experts

To identify the aspects for future improvement and learn the overall impression on the VeriMask platform, we collected feedback and suggestions from healthcare professionals, researchers in the field, and decontamination process experts through anonymous surveys. We received 21 answers from a pool that includes physicians, registered nurses, patient care technicians, sterile process managers, medical students, biomedical researchers, and faculty of medicine and engineering from various countries such as US, Italy, and China. Many of these were recruited from the collective of volunteers we worked with (anonymized). The interviewees were asked to give their impression on the VeriMask monitoring functionalities, the user interface, and the throughput optimization feature, and then provide suggestions on improving the overall capability of VeriMask based on their expertise.

VeriMask Functionality. While one interviewee points out that there is still operators' manual effort required to implement MH decontamination procedures in hospitals with VeriMask, 16/21 (76%) of interviewees strongly agreed or agreed that moist-heat decontamination integrated with the VeriMask platform can be recommended as an emergency procedure to decontaminate N95 masks for reuse in healthcare facilities facing mask shortage. The remaining three interviewees prefer expressing a neutral opinion. In addition, 14/21 (67%) of interviewees strongly agreed or agreed that VeriMask can help avoid insufficient decontamination or failures, 6/21 (28%) remain neutral, while one interviewee clarified the necessity of ensuring compliance with medical standards for masks handling under decontamination failure to avoid risk for the operators.

VeriMask User Interface. Almost all the interviewees (19/21 or 90%, with 2 neutral opinions on average among three questions) think the VeriMask smartphone application can greatly accelerate the manual inspection process and display information in a complete and easy-to-use manner. We also received positive feedback on the app's recommendations for the optimal heating device setup. One interviewee suggests instead the use of icons and pictures as a way to enhance the user experience.

Insight for Future Improvements. In addition to providing feedback on the platform, some interviewees suggest interesting insights into both improving VeriMask functionalities and enhancing integration with the clinical setting. One suggestion refers to the possibility of storing automatically multiple cycle information in the application. The current platform only allows the recording of a single decontamination cycle at the time by clicking a specific button. Recording multiple cycles while imply a more sophisticated memory management, can allow further post-decontamination analysis on the collected data and provide a backup record of the decontamination processes for the hospitals. Another suggestion consists in including different operational modes (e.g. automatic and advanced modes) in the application accordingly to different levels of user expertise. For instance, the automatic mode can be designed for ordinary operators for easy and fully automated verification. The advanced mode, on the other hand, can designed for experienced operators (e.g., doctors and nurses) to allow more personalized interactions such as setting more fine-grained decontamination parameters. This additional functionality requires more in-depth integration with the specific hospitals' internal policies and regulations (e.g.

credential management for different authorized operators) that can impact the generality-oriented design of the platform. Finally, other suggestions consist in providing user guides for the operators in addition to the open hardware implementation design to facilitate the adoption of VeriMask in different clinical settings, and further reducing the sensor node dimension to improve the overall portability.

7.2 Lessons Learned

Based on our experience, we now briefly summarize the lessons learned in the pandemic in the hope to help future researchers and designers to better safeguard the future. First, emergency designs should be prepared long in advance. Our team started developing VeriMask in response to the serious N95 mask shortages in US in mid 2020 [21] and had the first working prototype at the beginning of the 2021 when the shortage was already ramping down. We identify three major reasons of such need-response mismatch in emergency design for PPE shortage in pandemics: 1) The challenge of understanding the medical specification and standards which calls for collaborations with medical practitioners; 2) The challenge of getting access to clinics for design and testing due to stricter health regulations in pandemic times; 3) The challenge of disrupted supply and fabrication chains which seriously increases the hardware turn-around time. Our experience highlights the importance of getting prepared before crises happens, which are almost certain to happen again judging from the history of past pandemics [60, 100]. Second, designers should plan for the worst case and design for modularity. The problem of disrupted supply chain can not only delay fabrication, but also render the electronic components completely out-of-stock for months in pandemics. The designers should thus avoid assuming adequate supplies for emergency design, and even consider candidate components from design phase or leave spaces on PCBs for alternative components. Finally, designers should engage early with medical professionals and end users so that both mobile computing researchers and clinics are prepared and have a framework to build around. Our team has been in direct contact with the N95DECON consortium [89] which is a volunteer collective of scientists, engineers, clinicians, etc, and dedicates to studying different methods of decontamination. Our communications enabled more efficient and down-to-earth specification derivation which helped us avoid over-optimization and overlooking seemingly unrelated but actually important form factors that can greatly improve user experience.

8 CONCLUSION

In response to the shortage of N95 masks caused by the COVID-19 pandemic, we designed VeriMask—a wireless sensor platform that can verify and automate moist-heat decontamination processes of N95 masks. We design the highly scalable and flexible platform composed of low-power and low-cost sensor nodes that can reliably measure the temperature and relative humidity during the decontamination process, and an Android application to detect decontamination failures and increase decontamination throughput. We evaluated VeriMask in both a laboratory setting and in a real clinical scenario. Our results show that VeriMask can be widely and rapidly deployed in health-care facilities to help address the challenge of N95 masks shortages. From the experience of designing VeriMask we have defined the challenges, the design criteria, and the lesson learned in the process. Ultimately, we hope that the proposed design experience will help system designers and healthcare facilities formalize safe N95 masks decontamination procedures during future emergency crises to better protect front-line workers from the risk of infection from reused masks.

ACKNOWLEDGMENTS

This works is supported by NSF under the grants CNS-2031077, CNS-2032408, CNS-2107400, and a gift from Facebook. Any opinions, findings, and conclusions or recommendations expressed in this material are those of the authors and do not necessarily reflect the views of the National Science Foundation. The authors would also like to thank the reviewers for their incredibly helpful and constructive comments. We thank Weikun Lyu and

Connor Bolton for their valuable inputs. We express our sincere gratitude to the N95DECON consortium and the University of Michigan hospital.

REFERENCES

[1] 2015. 3M Technical Data Bulletin 171: Nanotechnology and Respirator Use. https://multimedia.3m.com/mws/media/376179O/nanotechnology-and-respirator-use.pdf.

[2] 2015. Honeywell HumidIcon™ Digital Humidity/Temperature Sensors HIH8000 Series. https://sensing.honeywell.com/index.php?ci_id=147072.

[3] 2015. STM32 Power shield, Nucleo expansion board for power consumption measurement. https://www.st.com/en/evaluation-tools/x-nucleo-lpm01a.html.

[4] 2016. Si7021-A20 I2C Humidity and Temperature Sensor. https://www.silabs.com/documents/public/data-sheets/Si7021-A20.pdf.

[5] 2018. SHT3x-DIS Humidity and Temperature Sensor. https://media.digikey.com/pdf/Data%20Sheets/Sensirion%20PDFs/HT_DS_SHT3x_DIS.pdf.

[6] 2019. Bluetooth Core Specifications. https://www.bluetooth.com/specifications/bluetooth-core-specification/.

[7] 2019. nRF52833 Objective Product Specification v0.7. https://infocenter.nordicsemi.com/pdf/nRF52833_OPS_v0.7.pdf.

[8] 2020. Android Developer Bluetooth Overview. https://developer.android.com/guide/topics/connectivity/bluetooth.

[9] 2020. Android Scan Settings. https://developer.android.com/reference/android/bluetooth/le/ScanSettings.

[10] 2020. APIC and N95DECON suggested guidance for infection prevention and workflow for UV-C decontamination of N95 FFRs during COVID-19. https://www.n95decon.org/files/apic-uvc.

[11] 2020. Covid-19: Indian healthcare workers need adequate PPE. https://blogs.bmj.com/bmj/2020/06/19/covid-19-indian-healthcare-workers-need-adequate-ppe/.

[12] 2020. Decontaminate N95 Respirators with Bioquell Technology. https://www.bioquell.com/n95/.

[13] 2020. Emergency Use Authorization granted to ASP STERRAD Systems to Enable Re-Use of N95 respirator. https://www.asp.com/blog/emergency-use-authorization-asp-re-use-n95-respirator.

[14] 2020. Example Return to Original User Setup and Logistics. https://www.n95decon.org/files/example-reprocessing-logistics.

[15] 2020. FDA Issues Warning Letter to Battelle Memorial Institute, a Manufacturer of an Authorized Decontamination System Used on Respirators. https://www.fda.gov/news-events/press-announcements/fda-issues-warning-letter-battelle-memorial-institute-manufacturer-authorized-decontamination-system.

[16] 2020. Health Care Workers Still Face Daunting Shortages of Masks and Other P.P.E. https://www.nytimes.com/2020/12/20/health/covid-ppe-shortages.html.

[17] 2020. Heat & Humidity: Example Validation and Operation. https://www.n95decon.org/files/n95decon-heat-humidity-example-protocol.

[18] 2020. Implementing Filtering Facepiece Respirator (FFR) Reuse, Including Reuse after Decontamination, When There Are Known Shortages of N95 Respirators. https://www.cdc.gov/coronavirus/2019-ncov/hcp/ppe-strategy/decontamination-reuse-respirators.html.

[19] 2020. N95 Decontamination & Reuse Methods Comparison Matrix. https://www.n95decon.org/files/comparison-matrix.

[20] 2020. N95 Respirators, Surgical Masks, and Face Masks. https://www.fda.gov/medical-devices/personal-protective-equipment-infection-control/n95-respirators-surgical-masks-and-face-masks.

[21] 2020. NPR Probes Why Personal Protective Equipment Is Still In Short Supply. https://www.npr.org/2020/09/16/913448230/npr-investigates-why-the-shortages-of-personal-protective-equipment.

[22] 2020. Online Power Profiler Tool For nRF52 Series SoCs. https://devzone.nordicsemi.com/nordic/power/w/opp/2/online-power-profiler-for-ble.

[23] 2020. Open-Source Medical Hardware: What You Should Know and What You Can Do. https://creativecommons.org/2020/04/15/open-source-medical-hardware-what-you-should-know-and-what-you-can-do/.

[24] 2020. PANDEMIC PLANNING: Recommended Guidance for Extended Use and Limited Reuse of N95 Filtering Facepiece Respirators in Healthcare Settings. https://www.cdc.gov/niosh/topics/hcwcontrols/recommendedguidanceextuse.html.

[25] 2020. Pentagon awards $415 million contract for units to decontaminate N95 masks. https://www.cnn.com/2020/04/13/politics/pentagon-n95-mask-decontamination/index.html.

[26] 2020. Recommendations for Sponsors Requesting EUAs for Decontamination and Bioburden Reduction Systems for Surgical Masks and Respirators During the Coronavirus Disease 2019 (COVID-19) Public Health Emergency Guidance for Industry and Food and Drug Administration Staff. https://www.fda.gov/media/138362/download.

[27] 2020. SensorPush Wireless Thermometer/Hygrometer . https://www.amazon.com/SensorPush-Wireless-Thermometer-Hygrometer-Android/dp/B01AEQ9X9I/.

[28] 2020. STERIS Decontamination Solutions for compatible N95 Respirators. https://www.steris.com/healthcare/steris-decontamination-solutions-for-compatible-n95-or-n95-equivalent-respirators.

[29] 2020. Survey Shows Nurses Still Having to Reuse PPE for COVID Patients. https://www.govtech.com/em/safety/Survey-Shows-Nurses-Still-Having-to-Reuse-PPE-for-COVID-Patients.html.
[30] 2020. Technical Report for Ethylene Oxide-Based N95 FFR Decontamination and Reuse. https://www.n95decon.org/files/ethylene-oxide-technical-report.
[31] 2020. Updates On Nurses And PPE. https://www.nursingworld.org/~4a558d/globalassets/covid19/ana-ppe-survey-one-pager---final.pdf.
[32] 2020. UV-C CABINET. https://static1.squarespace.com/static/5e8126f89327941b9453eeef/t/601b179dbe2f0b7fcd4e7491/1612388253557/UV-C_Educational_Infographic_English.pdf.
[33] 2020. What is Thermal Profiling? https://www.flukeprocessinstruments.com/en-us/service-and-support/knowledge-center/thermal-profiling-technology/what-thermal-profiling%3F.
[34] 2021. Department of Internal Trade seeks to avert mask shortage. https://www.bangkokpost.com/thailand/general/2110307/department-of-internal-trade-seeks-to-avert-mask-shortage.
[35] 2021. More experts now recommend medical masks. Good ones are hard to find. https://www.washingtonpost.com/health/2021/02/02/medical-mask-shortage/.
[36] 2021. Stitching Together a Solution: Lessons from the Open Source Hardware Response to COVID-19. https://www.law.nyu.edu/sites/default/files/stitching-together-a-solution-202102.pdf.
[37] 2021. Underpaid and overworked, Philippine nurses would rather walk away than work at home. https://www.channelnewsasia.com/news/cnainsider/underpaid-overworked-philippines-nurses-hospitals-shortage-covid-14640028.
[38] 2021. 'Sari is my mask': How the COVID pandemic has hit India's poorest. https://www.aljazeera.com/news/2021/5/5/sari-is-my-mask-how-the-pandemic-has-hit-indias-poorest.
[39] Loïc Anderegg, John Doyle, Margaret L Gardel, Amit Gupta, Christian Hallas, Yuri Lensky, Nancy G Love, Bronwyn A Lucas, Edward Mazenc, Cole Meisenhelder, et al. 2021. Heat and Humidity for Bioburden Reduction of N95 Filtering Facepiece Respirators. *Applied Biosafety* (2021).
[40] Boyd Anderson, Mingqian Shi, Vincent YF Tan, and Ye Wang. 2019. Mobile Gait Analysis Using Foot-Mounted UWB Sensors. *Proceedings of the ACM on Interactive, Mobile, Wearable and Ubiquitous Technologies* 3, 3 (2019), 1–22.
[41] Kenneth Bannister, Gianni Giorgetti, and SK Gupta. 2008. Wireless sensor networking for hot applications: Effects of temperature on signal strength, data collection and localization. In *Proceedings of the 5th Workshop on Embedded Networked Sensors (HotEmNets' 08)*. Citeseer, 1–5.
[42] Norberto Barroca, Luís M Borges, Fernando J Velez, Filipe Monteiro, Marcin Górski, and João Castro-Gomes. 2013. Wireless sensor networks for temperature and humidity monitoring within concrete structures. *Construction and Building Materials* 40 (2013), 1156–1166.
[43] Emmanuel J Candes and Yaniv Plan. 2010. Matrix completion with noise. *Proc. IEEE* 98, 6 (2010), 925–936.
[44] Irene O Carrillo, Anna CE Floyd, Christian M Valverde, Travis N Tingle, and Firas R Zabaneh. 2020. Immediate-use steam sterilization sterilizes N95 masks without mask damage. *Infection Control & Hospital Epidemiology* 41, 9 (2020), 1104–1105.
[45] James K Carson, Jim Willix, and Mike F North. 2006. Measurements of heat transfer coefficients within convection ovens. *Journal of Food Engineering* (2006).
[46] Jie Cheng, Qiang Ye, Hongbo Jiang, Dan Wang, and Chonggang Wang. 2012. STCDG: An efficient data gathering algorithm based on matrix completion for wireless sensor networks. *IEEE Transactions on Wireless Communications* 12, 2 (2012), 850–861.
[47] Lucia Corsini, Valeria Dammicco, and James Moultrie. 2020. Critical Factors for Implementing Open Source Hardware in a Crisis: Lessons Learned from the COVID-19 Pandemic. *Journal of Open Hardware* 4, 1 (2020).
[48] Simeon C Daeschler, Niclas Manson, Kariym Joachim, Alex WH Chin, Katelyn Chan, Paul Z Chen, Kiana Tajdaran, Kaveh Mirmoeini, Jennifer J Zhang, Jason T Maynes, et al. 2020. Effect of moist heat reprocessing of N95 respirators on SARS-CoV-2 inactivation and respirator function. *CMAJ* (2020).
[49] Artem Dementyev, Steve Hodges, Stuart Taylor, and Joshua Smith. 2013. Power consumption analysis of Bluetooth Low Energy, ZigBee and ANT sensor nodes in a cyclic sleep scenario. In *2013 IEEE International Wireless Symposium (IWS)*. IEEE, 1–4.
[50] Elena Di Lascio, Shkurta Gashi, Juan Sebastian Hidalgo, Beatrice Nale, Maike E Debus, and Silvia Santini. 2020. A Multi-Sensor Approach to Automatically Recognize Breaks and Work Activities of Knowledge Workers in Academia. *Proceedings of the ACM on Interactive, Mobile, Wearable and Ubiquitous Technologies* 4, 3 (2020), 1–20.
[51] Hamid Farahani, Rahman Wagiran, and Mohd Nizar Hamidon. 2014. Humidity sensors principle, mechanism, and fabrication technologies: a comprehensive review. *Sensors* (2014).
[52] Anthony Ferrese. 2015. Battery Fundamentals. *GetMobile: Mobile Computing and Communications* 19, 3 (2015), 29–32.
[53] Centers for Disease Control, Prevention, et al. 2018. Public health emergency preparedness and response capabilities: National standards for state, local, tribal, and territorial public health. *Atlanta, GA: US Department of Health and Human Services* (2018).
[54] Centers for Disease Control, Prevention, et al. 2020. Management of visitors to healthcare facilities in the context of COVID-19: non-US healthcare settings. *Atlanta, GA: US Department of Health and Human Services, CDC* (2020).

[55] Hemant Ghayvat, Subhas Mukhopadhyay, Xiang Gui, and Nagender Suryadevara. 2015. WSN-and IOT-based smart homes and their extension to smart buildings. *Sensors* 15, 5 (2015), 10350–10379.
[56] Adam Golda and Andrzej Kos. 2003. Temperature influence on power consumption and time delay. In *Euromicro Symposium on Digital System Design, 2003. Proceedings.* IEEE, 378–382.
[57] Samantha M Grist, Alisha Geldert, Anjali Gopal, Alison Su, Halleh B Balch, Amy E Herr, and N95DECON Consortium. 2021. Current Understanding of Ultraviolet-C Decontamination of N95 Filtering Facepiece Respirators. *Applied Biosafety* (2021).
[58] Manik Grover, Suraj Kumar Pardeshi, NirbhowJap Singh, and Sanjay Kumar. 2015. Bluetooth low energy for industrial automation. In *2015 2nd International Conference on Electronics and Communication Systems (ICECS).* IEEE, 512–515.
[59] Sanjeev Kumar Gupta and Poonam Sinha. 2014. Overview of wireless sensor network: a survey. *Telos* (2014).
[60] Mayuko Hashikura and Junko Kizu. 2009. Stockpile of personal protective equipment in hospital settings: preparedness for influenza pandemics. *American journal of infection control* 37, 9 (2009), 703–707.
[61] B Heimbuch and D Harnish. 2019. Research to Mitigate a Shortage of Respiratory Protection Devices During Public Health Emergencies. *Applied Research Associates* (2019).
[62] Alfredo Herrera. 2020. The Promises and Challenges of Open Source Hardware. *IEEE Annals of the History of Computing* 53, 10 (2020), 101–104.
[63] Natsuki Ikeda, Ryo Shigeta, Junichiro Shiomi, and Yoshihiro Kawahara. 2020. Soil-Monitoring Sensor Powered by Temperature Difference between Air and Shallow Underground Soil. *Proceedings of the ACM on Interactive, Mobile, Wearable and Ubiquitous Technologies* 4, 1 (2020), 1–22.
[64] Seyran Khademi, Sundeep Prabhakar Chepuri, Zoubir Irahhauten, Gerard JM Janssen, and Alle-Jan van der Veen. 2015. Channel measurements and modeling for a 60 GHz wireless link within a metal cabinet. *IEEE Transactions on Wireless Communications* 14, 9 (2015), 5098–5110.
[65] Yoojung Kim, Hee-Tae Jung, Joonwoo Park, Yangsoo Kim, Nathan Ramasarma, Paolo Bonato, Eun Kyoung Choe, and Sunghoon Ivan Lee. 2019. Towards the Design of a Ring Sensor-based mHealth System to Achieve Optimal Motor Function in Stroke Survivors. *Proceedings of the ACM on Interactive, Mobile, Wearable and Ubiquitous Technologies* 3, 4 (2019), 1–26.
[66] Patrick Kirchner, Jan Oberländer, Henri-Pierre Suso, Gunnar Rysstad, Michael Keusgen, and Michael J Schöning. 2013. Towards a wireless sensor system for real-time H2 O 2 monitoring in aseptic food processes. *physica status solidi (a)* 210, 5 (2013), 877–883.
[67] Mustafa Kocakulak and Ismail Butun. 2017. An overview of Wireless Sensor Networks towards internet of things. In *2017 IEEE 7th annual computing and communication workshop and conference (CCWC).* IEEE, 1–6.
[68] Douglas S Kridi, Carlos Giovanni N de Carvalho, and Danielo G Gomes. 2016. Application of wireless sensor networks for beehive monitoring and in-hive thermal patterns detection. *Computers and Electronics in Agriculture* 127 (2016), 221–235.
[69] Gierad Laput and Chris Harrison. 2019. Exploring the efficacy of sparse, general-purpose sensor constellations for wide-area activity sensing. *Proceedings of the ACM on Interactive, Mobile, Wearable and Ubiquitous Technologies* 3, 2 (2019), 1–19.
[70] Lauren E Linderman, Jennifer A Rice, Suhail Barot, Billie F Spencer Jr, and Jennifer T Bernhard. 2010. Characterization of wireless smart sensor performance. *Journal of engineering mechanics* 136, 12 (2010), 1435–1443.
[71] Yumei Liu, Changli Zhang, and Ping Zhu. 2011. The temperature humidity monitoring system of soil based on wireless sensor networks. In *2011 International Conference on Electric Information and Control Engineering.* IEEE, 1850–1853.
[72] Mir Lodro, Chris Smart, Gabriele Gradoni, Ana Vukovic, Dave Thomas, and Steve Greedy. 2020. Near-field BER and EVM Measurement at 5.8 GHz in Mode-stirred Metal Enclosure. *Applied Computational Electromagnetics Society Journal* 35, 9 (2020).
[73] Michael B Lore, Brian K Heimbuch, Teanne L Brown, Joseph D Wander, and Steven H Hinrichs. 2012. Effectiveness of three decontamination treatments against influenza virus applied to filtering facepiece respirators. *Annals of occupational hygiene* (2012).
[74] Jari Luomala and Ismo Hakala. 2015. Effects of temperature and humidity on radio signal strength in outdoor wireless sensor networks. In *2015 Federated Conference on Computer Science and Information Systems (FedCSIS).* IEEE, 1247–1255.
[75] A Maia Chagas, JC Molloy, LL Prieto Godino, and T Baden. 2020. Leveraging Open Hardware to Alleviate the Burden of COVID-19 on Global Health Systems. *PLoS Biology* (2020).
[76] Andre Maia Chagas, Jennifer C Molloy, Lucia L Prieto-Godino, and Tom Baden. 2020. Leveraging open hardware to alleviate the burden of COVID-19 on global health systems. *PLoS biology* 18, 4 (2020), e3000730.
[77] Mohammad Abdul Matin and MM Islam. 2012. Overview of wireless sensor network. *Wireless sensor networks-technology and protocols* (2012), 1–3.
[78] Hitesh Mistry, Subhrajit Dey, Peeush Bishnoi, Jose Luis Castillo, et al. 2006. Modeling of transient natural convection heat transfer in electric ovens. *Applied thermal engineering* (2006).
[79] Dylan H Morris, Kwe Claude H Yinda, Amandine Gamble, Fernando W Rossine, Qishen Huang, Trenton Bushmaker, Robert J Fischer, M Jeremiah Matson, Neeltje van Doremalen, Peter J Vikesland, et al. 2020. The effect of temperature and humidity on the stability of SARS-CoV-2 and other enveloped viruses. *bioRxiv* (2020).
[80] P Navaneethakrishnan, PSS Srinivasan, and S Dhandapani. 2010. Numerical and experimental investigation of temperature distribution inside a heating oven. *Journal of food processing and preservation* (2010).

[81] Gerrit Niezen, Parisa Eslambolchilar, and Harold Thimbleby. 2016. Open-source hardware for medical devices. *BMJ innovations* 2, 2 (2016).
[82] Maciej Nikodem and Marek Bawiec. 2020. Experimental Evaluation of Advertisement-Based Bluetooth Low Energy Communication. *Sensors* 20, 1 (2020), 107.
[83] WM Nooriman, AH Abdullah, N Abdul Rahim, and K Kamarudin. 2018. Development of wireless sensor network for Harumanis Mango orchard's temperature, humidity and soil moisture monitoring. In *2018 IEEE Symposium on Computer Applications & Industrial Electronics (ISCAIE)*. IEEE, 263–268.
[84] World Health Organization et al. 2017. Emergency response framework (ERF). (2017).
[85] Guntur Dharma Putra, Azkario Rizky Pratama, Alexander Lazovik, and Marco Aiello. 2017. Comparison of energy consumption in Wi-Fi and bluetooth communication in a Smart Building. In *2017 IEEE 7th Annual Computing and Communication Workshop and Conference (CCWC)*. IEEE, 1–6.
[86] Meera Radhakrishnan, Archan Misra, Rajesh Krishna Balan, and Youngki Lee. 2015. Smartphones and ble services: Empirical insights. In *2015 IEEE 12th International Conference on Mobile Ad Hoc and Sensor Systems*. IEEE, 226–234.
[87] V Rajaravivarma, Yi Yang, and Teng Yang. 2003. An overview of wireless sensor network and applications. In *Proceedings of the 35th Southeastern Symposium on System Theory, 2003*. IEEE, 432–436.
[88] Haroon Rashid, Sanjana Mendu, Katharine E Daniel, Miranda L Beltzer, Bethany A Teachman, Mehdi Boukhechba, and Laura E Barnes. 2020. Predicting Subjective Measures of Social Anxiety from Sparsely Collected Mobile Sensor Data. *Proceedings of the ACM on Interactive, Mobile, Wearable and Ubiquitous Technologies* 4, 3 (2020), 1–24.
[89] David Rempel. 2020. Scientific Collaboration During the COVID-19 Pandemic: N95DECON. org. *Annals of Work Exposures and Health* (2020).
[90] David Rempel, John Henneman, James Agalloco, Jill Crittenden, and N95DECON Consortium. 2020. Hydrogen Peroxide Methods for Decontaminating N95 Filtering Facepiece Respirators. *Applied Biosafety* (2020).
[91] Annika Richterich. 2020. When open source design is vital: critical making of DIY healthcare equipment during the COVID-19 pandemic. *Health Sociology Review* 29, 2 (2020), 158–167.
[92] Nicole Rockey, Peter J Arts, Lucinda Li, Katherine R Harrison, Kathryn Langenfeld, William J Fitzsimmons, Adam S Lauring, Nancy G Love, Keith S Kaye, Lutgarde Raskin, et al. 2020. Humidity and deposition solution play a critical role in virus inactivation by heat treatment on N95 respirators. *medRxiv* (2020).
[93] Carlos E Rodriguez-Martinez, Monica P Sossa-Briceño, and Jorge A Cortés-Luna. 2020. Decontamination and reuse of N95 filtering facemask respirators: a systematic review of the literature. *American journal of infection control* (2020).
[94] Luis Ruiz-Garcia, Loredana Lunadei, Pilar Barreiro, and Ignacio Robla. 2009. A review of wireless sensor technologies and applications in agriculture and food industry: state of the art and current trends. *Sensors* 9, 6 (2009), 4728–4750.
[95] N. Saeed, M. Alouini, and T. Y. Al-Naffouri. 2019. Toward the Internet of Underground Things: A Systematic Survey. *IEEE Communications Surveys Tutorials* 21, 4 (2019), 3443–3466.
[96] Maikon Lorran Santos, Leonardo Rakauskas Zacharias, and Vinícius Rosa Cota. 2021. Open-source hardware to face COVID-19 pandemic: the need to do more and better. *Research on Biomedical Engineering* (2021), 1–12.
[97] Gaoyang Shan, Byeong-uk Lee, Seung-Hun Shin, and Byeong-hee Roh. 2017. Design and implementation of simulator for analysis of BLE broadcast signal collision. In *2017 International Conference on Information Networking (ICOIN)*. IEEE, 448–452.
[98] E Sisinni, A Depari, and A Flammini. 2016. Design and implementation of a wireless sensor network for temperature sensing in hostile environments. *Sensors and Actuators A: Physical* (2016).
[99] Abbas Tcharkhtchi, N Abbasnezhad, M Zarbini Seydani, N Zirak, S Farzaneh, and Mohammadali Shirinbayan. 2020. An overview of filtration efficiency through the masks: Mechanisms of the aerosols penetration. *Bioactive materials* 6, 1 (2020), 106–122.
[100] Taro Tomizuka, Yasuhiro Kanatani, and Kazuo Kawahara. 2013. Insufficient preparedness of primary care practices for pandemic influenza and the effect of a preparedness plan in Japan: a prefecture-wide cross-sectional study. *BMC family practice* 14, 1 (2013), 1–9.
[101] Dennis J Viscusi, Michael S Bergman, Benjamin C Eimer, and Ronald E Shaffer. 2009. Evaluation of five decontamination methods for filtering facepiece respirators. *Annals of occupational hygiene* (2009).
[102] Stuart J Williams. 2020. Assessment of a Food-Warming Cabinet for Heat and Humidity Decontamination of N95 Respirators. *Journal of Heat Transfer* (2020).
[103] Myung-Heui Woo, Adam Grippin, Diandra Anwar, Tamara Smith, Chang-Yu Wu, and Joseph D Wander. 2012. Effects of relative humidity and spraying medium on UV decontamination of filters loaded with viral aerosols. *Applied and environmental microbiology* (2012).